The photosensitive phase acts as a sensitive window for seasonal multisensory neuroplasticity in male and female starlings

Jasmien Orije[1], Emilie Cardon[1], Julie Hamaide[1], Elisabeth Jonckers[1], Veerle M. Darras[2], Marleen Verhoye[1], Annemie Van der Linden[1]

1 Bio-Imaging Lab, University of Antwerp, Belgium

2 Laboratory of Comparative Endocrinology, Biology Department, KU Leuven, Belgium

Abstract

Traditionally, research unraveling seasonal neuroplasticity in songbirds has focused on the male song control system and testosterone. We longitudinally monitored the song and neuroplasticity in male and female starlings during multiple photoperiods using Diffusion Tensor and Fixel-Based techniques. These exploratory data-driven whole-brain methods resulted in a population-based tractogram uncovering microstructural sexual dimorphisms in the song control system and beyond. Male brains showed microstructural hemispheric asymmetries, whereas females had higher interhemispheric connectivity, which could not be attributed to brain size differences. Only females with large brains sing but differ from males in their song behavior by showing involvement of the hippocampus. Both sexes experienced multisensory neuroplasticity in the song control, auditory and visual system, and the cerebellum, mainly during the photosensitive period. This period with low gonadal hormones might represent a 'sensitive window' during which different sensory and motor systems in telencephalon and cerebellum can be seasonally re-shaped in both sexes.

1 ABBREVIATIONS

A	Arcopallium
AD	Axial diffusivity
CA	*Commisura anterior* / anterior commissure
CbL	*Nucleus cerebellaris lateralis* / lateral cerebellar nucleus
CO	*Chiasma opticum* / optic chiasm
CP	*Commisura posterior* / posterior commissure
CSt	Caudal part of the lateral striatum
DLM	*Nucleus dorsolateralis anterior thalami pars medialis* / medial part of the dorsolateral nucleus of the anterior thalamus
DMA	Dorsomedial nucleus of the anterior thalamus
DMP	Dorsomedial nucleus of the posterior thalamus

DSD	*Decussatio supraoptica dorsalis*
E	Entopallium
FA	Fractional anisotropy
FC	Fiber-bundle cross-section
FD	Fiber density
FOD	Fiber orientation distribution
FPL	*Fasciculus prosencephali lateralis* / lateral forebrain bundle
GP	Globus pallidus
HA	*Hyperpallium apicale* / apical part of the hyperpallium
HD	*Hyperpallium densocellulare* / densocellular part of the hyperpallium
HVC	Used as a proper name (High vocal center)
LAD	*Lamina arcopallialis dorsalis* / dorsal arcopallial lamina
LaM	*Lamina mesopallialis* / mesopallial lamina
LFM	*Lamina frontalis suprema* / supreme frontal lamina
LFS	*Lamina frontalis superior* / superior frontal lamina
LMAN	*Nucleus lateralis magnocellularis nidopallii anterioris* / lateral magnocellular nucleus of the anterior nidopallium
LPS	*Lamina pallio-subpallialis* / pallial-subpallial lamina
LSt	*Striatum laterale* / lateral striatum
M	Mesopallium
MD	Mean diffusivity
MLD-DM-ICO	Intercollicular nucleus complex
MMAN	*Nucleus medialis magnocellularis nidopallii anterioris* / medial magnocellular nucleus of the anterior nidopallium
MRI	Magnetic Resonance Imaging
MSt	*Striatum mediale* / medial striatum
N	Nidopallium
NCM	*Nidopallium caudomediale* / caudomedial nidopallium
OM	*Tractus occipito-mesencephalicus* / occipito-mesencephalic tract
Ov	Nucleus ovoidalis
POA	*Area praeoptica* / pre-optic area
Pt	*Nucleus pretectalis* / pretectal nucleus
RA	*Nucleus robustus arcopallialis* / robust nucleus of arcopallium
RARE	Rapid acquisition with relaxation enhancement
RD	Radial diffusivity
Rt	*Nucleus rotundus*
surr	*surroundings*
TeO	*Tectum opticum* / optic tectum
tFA	*Tractus fronto-arcopallialis* / fronto-arcopallial tract
TFM	*Tractus thalamo-frontalis*
TnA	*Nucleus taeniae amygdalae* / nucleus taeniae of the amygdala
TrO	*Tractus opticus* / optic tract
TSM	*Tractus septopallio-mesencephalicus* / septopallio-mesencephalic tract

23

2 INTRODUCTION

24

25 Although various songbird species demonstrate different levels of female song, in one of the most

26 studied song bird species, the zebra finch, female song is absent (Odom et al., 2014). Observations like

27 these led to the discovery of one of the largest sexual dimorphisms in the brain of vertebrate species

28 (Bernard et al., 1993; Nottebohm and Arnold, 1976). Such sexual dimorphisms in singing behavior and

29 brain structure drove a bias in research of the song control system towards male songbirds. Besides

30 the large sexual dimorphism in song and song control nuclei, seasonal songbirds expose an additional

31 peculiarity as they display naturally re-occurring seasonal cycles of singing and neuroplasticity of the

32 song control system. However, the male focus proceeded in the research of seasonal neuroplasticity,

33 since this process was shown to be largely driven by photoperiod-induced increases in testosterone,

34 which results in a pre-optic area (POA) mediated increase in motivation to sing and subsequent singing

35 activity induced neuroplasticity (Alward et al., 2013). The largest differences in song control nuclei

36 volumes are found between breeding and non-breeding season (Riters et al., 2002). This led seasonal

37 neuroplasticity studies to focus mainly on the breeding season or photostimulated phase, which they

38 often compare to the non-breeding season or photorefractory and photosensitive phases. The main

39 emphasis on the role of photoperiodic-induced increase in testosterone has led to many manipulation

40 studies involving castration and/or testosterone implantation and its effect on song production and

41 the song control system (e.g. (Hall and Macdougall-Shackleton, 2012; Orije et al., 2020; Stevenson and
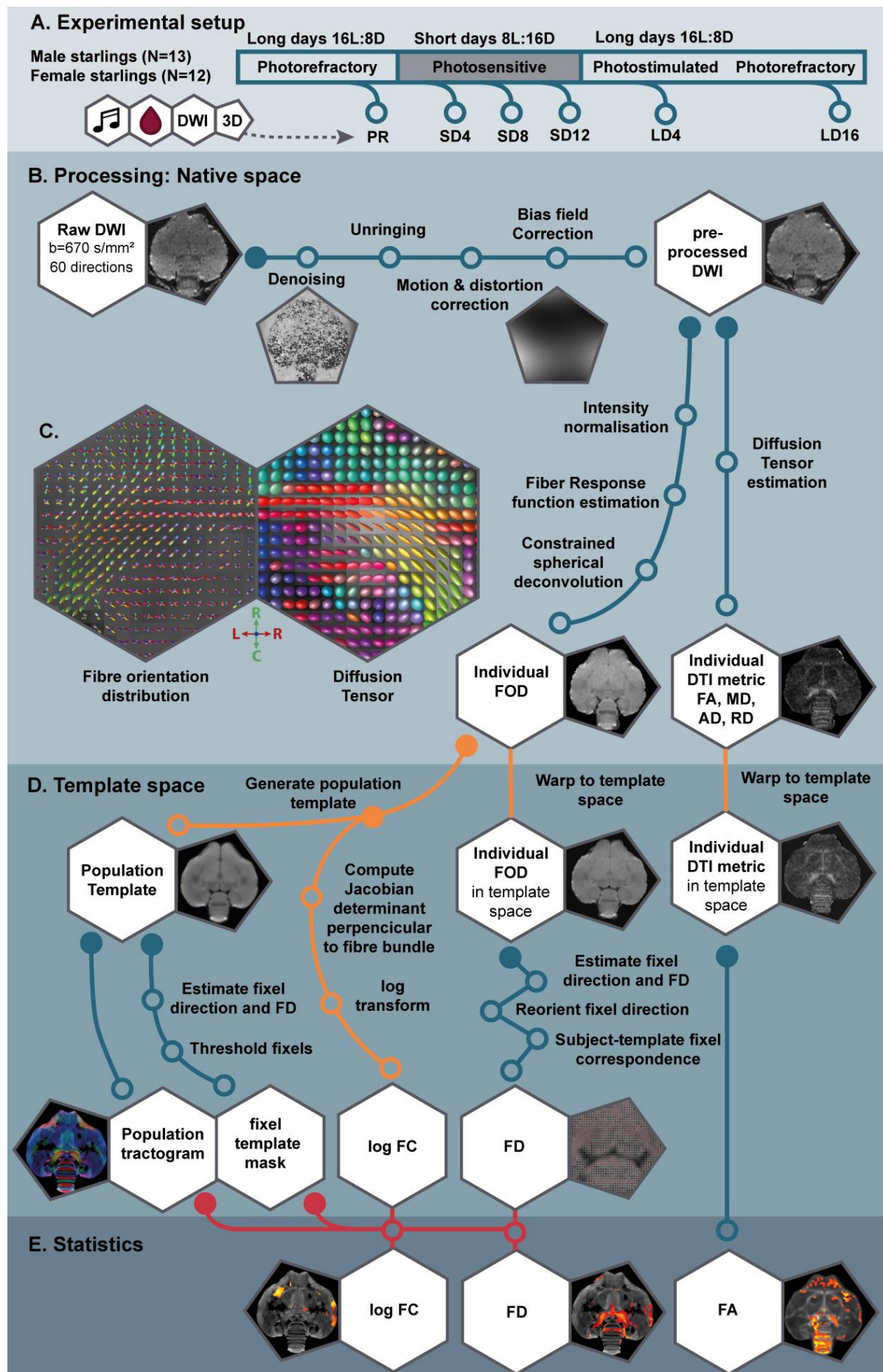
42 Ball, 2010)).

43 Prior studies have also pointed out that testosterone implants only have an effect when the birds have

44 experienced a photosensitive phase with short day length exposure (Bernard and Ball, 1997; Rouse et

45 al., 2015). Although little research is devoted to brain neuroplasticity during this state (Larson et al.,

46 2019; Riters et al., 2002), multiple studies have shown that during the photosensitive period, testes

47 size (Cornez et al., 2017) and GnRH expression in the POA slowly start to increase (Bentley et al., 2013;

48 Hurley et al., 2008; Stevenson et al., 2012), while some song control nuclei slowly start to grow (Riters

49 et al., 2002). The photosensitive period might be seen as a sensitive window, defined as a period in

50 which experiences lead to long-lasting changes (that remain in the subsequent photostimulated phase

51 or breading season) in the brain and song behavior (Knudsen, 2004). The photosensitive period plays

52 a crucial role in creating permissive circumstances for enhanced neuroplasticity resulting in enlarged

53 song control nuclei as observed during the photostimulated stage.

54 The studies on sexual dimorphisms and seasonal neuroplasticity in songbirds have been preoccupied

55 with vocal control areas as the neural substrate for the behavioral sexual dimorphism in song

56 performance. However, *in vivo* Magnetic Resonance Imaging (MRI) studies from our team focusing on

3

57   the entire songbird brain have demonstrated seasonal neuroplasticity and functional changes in both
58   auditory and olfactory systems of starlings (De Groof et al., 2017; De Groof et al., 2010; De Groof et
59   al., 2013). This outcome hints towards a seasonal re-occurring cycle of multisensory neuroplasticity
60   and raises the question whether the photosensitive stage perhaps represents a renewed 'sensitive
61   window' for heightened neuroplasticity and rewiring of various sensory and sensorimotor systems.

62   The current study aims to fill the gaps highlighted above and answers the following questions with an
63   extensive data-driven exploratory brain-wide structural MRI study of both male and female starlings
64   throughout different seasons: (1) Is **sexual dimorphism** limited to the song control system in starlings,
65   as in zebra finches where only the male sings (Hamaide et al., 2017) or does this dimorphism extend
66   to other sensory systems? Can it be attributed to a difference in total brain size between the sexes,
67   similar to what has been observed in mammals? (2) Do female and male starlings display parallel or
68   different **seasonal structural neuroplasticity**? Is this neuroplasticity limited to the song control system
69   or does it extend to other neural circuits? When do these (neuroplasticity) changes take place, already
70   during the photosensitive period when gonadal hormone levels are still very low? (3) How does
71   seasonal neuroplasticity correlate -at the group and individual level - with **gonadal hormone levels**
72   **and with song-production**?

73   Since MRI is an *in vivo* method, we were able to measure the same subjects repeatedly and monitor
74   the structural neuroplasticity longitudinally in thirteen male and twelve female starlings as they
75   undergo different subsequent photoperiodic phases: at baseline photorefractory state (PR), after four,
76   eight and twelve weeks of short days during the photosensitive state (SD4, SD8, SD12), after four
77   weeks of photostimulation (LD4) and after sixteen weeks on long days when the birds are
78   photorefractory again (LD16) (figure 1A). At each time point we: collected blood samples; measured
79   body weight; recorded song; and acquired structural MRI data including 3D anatomical scans and
80   diffusion-weighted images (DWI). Using voxel-based diffusion tensor imaging (DTI) and fixel-based
81   analysis (De Groof et al., 2006; Raffelt et al., 2017), we established spatio-temporal statistical maps
82   revealing microstructural changes in grey and white matter, specifically in fiber connections
83   throughout the different seasons in the entire brain in both sexes. To learn about the contribution of
84   singing activity induced neuroplasticity in the seasonal neuroplasticity, voxel-based multiple
85   regression between seasonal song rate and corresponding DTI parameter maps was performed to
86   identify the neuronal correlates of song behavior in both sexes (Hamaide et al., 2020; Sagi et al., 2012).

A. Experimental setup

Male starlings (N=13)
Female starlings (N=12)

Long days 16L:8D — Photorefractory
Short days 8L:16D — Photosensitive
Long days 16L:8D — Photostimulated — Photorefractory

PR · SD4 · SD8 · SD12 · LD4 · LD16

B. Processing: Native space

Raw DWI b=670 s/mm² 60 directions

Denoising · Unringing · Motion & distortion correction · Bias field Correction · pre-processed DWI

C.

Fibre orientation distribution · Diffusion Tensor

Intensity normalisation · Fiber Response function estimation · Constrained spherical deconvolution · Diffusion Tensor estimation

Individual FOD · Individual DTI metric FA, MD, AD, RD

D. Template space

Generate population template · Warp to template space · Warp to template space

Population Template

Compute Jacobian determinant perpencicular to fibre bundle

Individual FOD in template space · Individual DTI metric in template space

Estimate fixel direction and FD · log transform · Estimate fixel direction and FD · Reorient fixel direction · Subject-template fixel correspondence

Estimate fixel direction and FD · Threshold fixels

Population tractogram · fixel template mask · log FC · FD

E. Statistics

log FC · FD · FA

87

5

88 **Figure 1.** **Simplified overview of the experimental setup and various processing steps of the DTI and**

89 **fixel-based analysis. (A)** Male and female starlings were measured repeatedly as they went through

90 different photoperiods. At each time point, their songs were recorded, blood samples were collected

91 and T2-weighted 3D anatomical and diffusion-weighted images (DWI) were acquired. The 3D

92 anatomical images were used to extract whole-brain volume. (B) Using the DWI, we performed a

93 common DTI analysis and a fixel-based analysis. By doing this, the extracted DTI metrics (such as

94 fractional anisotropy (FA)) and fixel-based metrics (fiber density (FD) and fiber-bundle cross-section

95 (FC)) complemented each other during interpretation of the results. Insets present an example DWI

96 image at each respective processing step. (C) Large insets are at the level of the commisura anterior

97 and OM tract and show the fiber orientation distribution (FOD) and Diffusion Tensor map used in fixel-

98 based and DTI-based analysis respectively as described in table 1 collored according to the standard

99 red-green-blue code (red = left-right orientation (L-R), blue = dorso-ventral (D-V) and green = rostro-

100 caudal (R-C)). (D) All measures were normalized to a population template, a population-based

101 tractogram and fixel template mask were created which are necessary for the voxel- and fixel-based

102 statistical analysis (E). The material and method section contains the extended explanation on the

103 various processing steps. Abreviations: LD, long days; PR, photorefractory state; SD short days.
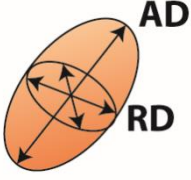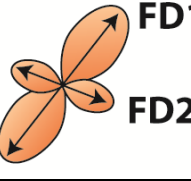
104 3 RESULTS

105 3.1 POPULATION-BASED TRACTOGRAM OF THE STARLING BRAIN USING FIXEL-BASED ANALYSIS

106 In the current study, we analyzed the DWI scans in two distinct ways: 1) using the common approach

107 of diffusion tensor derived metrics such as fractional anisotropy (FA) and; 2) using a novel method **of**

108 **fiber orientation distribution (FOD)** derived fixel-based analysis. Both techniques infer the

109 microstructural information based on the diffusion of water molecules, but they are conceptually

110 different (table 1). Figure 1B-E gives a comprehensive overview of the processing steps (see material

111 and method section for detailed outline). Common DTI analysis estimates for each voxel the diffusion

112 tensor from which several parameters can be extracted, which are sensitive to various microstructural

113 changes specified in table 1. Since this is a brain-wide voxel-based method, both white and grey matter

114 can be investigated. Fixel-based analysis on the other hand relies on a population-based tractogram

115 generated from FOD information and is therefore inherently sensitive only to changes in white matter

116 structures; both microscopic changes in apparent fiber density (FD) or macroscopic changes in fiber-

117 bundle cross-section (FC) (table 1). As a voxel can hold multiple fiber bundles, FD is estimated by the

118 intensity of the FOD before reorientation for each fiber bundle separately (illustrated by FD1 and FD2

119 in table 1). This allowed us to examine crossing fibers within a voxel, which is a major advantage of

120   the fixel-based analysis. FC is based on the transformation parameters or Jacobian determinants

121   perpendicular to the fixel orientation. For group statistical analysis, the FC values were logarithmically

122   transformed to log FC in order to center the data on zero and ensure a normal distribution. Positive

123   values indicate expansion, whereas negative values reflect shrinkage of a fiber bundle relative to the

124   template (Raffelt et al., 2017).

125   **Table 1. Overview of the parameters studied by common DTI analysis and novel fixel-based analysis,**

126   **including a comprehensive, but not exhaustive, list of some of the microstructural changes to which**

127   **they are sensitive.**

|	Metric	Level	Para-meter	Measures	Sensitive to changes in :
DTI analysis	Diffusion tensor	Voxel	FA	Directionality of water diffusion	Axon number and density, axon diameter, myelination, fiber organization
			MD	Average diffusion across all directions	Cell size, cell spacing, cell density, dendrite branching, extracellular space
			AD	Diffusion along the fiber direction	Axon number and density
			RD	Diffusion perpendicular to the fiber direction	Axon diameter and myelination
fixel-based analysis	Fiber orientation distribution	Fixel	FD	Microscopic density within fiber population	Axon number and density, axon diameter
			FC	Macroscopic change in cross-sectional area perpendicular to fiber bundle	Fiber bundle size due to changes in extra-axonal space and/or myelination, number of axons

128   Abbreviations: FA, fractional anisotropy; MD, mean diffusivity; AD, axial diffusivity; RD, radial

129   diffusivity; FD, fiber density; FC, fiber-bundle cross-section. Fixel-based analysis can distinguish

130   between different fiber bundles within a voxel and estimate FD for each fiber bundle separately (FD1

131   and FD2). For a complete description and interpretation of these measures we refer to the following

132   reviews of DTI analysis (Beaulieu, 2002; Beaulieu, 2014; Song et al., 2002; Zatorre et al., 2012) and

133   fixel based analysis (Genc et al., 2020; Raffelt et al., 2017)

134   It is important to note that fixel-based analysis was mainly created to study the human or mammalian

135   brain. The mammalian cortex has a laminar organization with large white matter tracts

136   interconnecting both hemispheres through the corpus callosum, whereas the avian telencephalon has

137   a nuclear organization with distinct white matter tracts organized in lamina (Jarvis et al., 2005). Avian

138   interhemispheric connections run mainly through the commissure anterior and posterior, as the

139   corpus callosum is an exclusively mammalian feature (Suarez et al., 2018). Certain connections

7

140   between avian nuclei cross the grey matter like pallium and organize in bundles such as the HVC-RA

141   tract (Karten et al., 2013). Since the connections within the avian brain are not organized in large white

142   matter tracts, but in lamina and sparse fibers crossing brain structures, a lower FOD threshold is

143   applied to ensure continuity in our fiber tracking. This holds the potential risk of introducing noisy

144   fixels, especially within the grey matter, which we will keep in mind during interpretation of the

145   results. However, a higher threshold may exclude many of the genuine white matter tracts, which is

146   unfavorable. The result is a population-based template in which many of the avian anatomical

147   structures can be identified (figure 2). We recognize many of the white matter structures such as the

148   different lamina, occipito-mesencephalic tract (OM) and optic tract (TrO) among others. Interestingly,

149   many of the nuclei within the song control system (i.e. HVC, robust nucleus of the arcopallium (RA),

150   lateral magnocellular nucleus of the anterior nidopallium (LMAN), and Area X), auditory system (i.e.

151   intercollicular nucleus complex, nucleus ovoidalis) and visual system (i.e. entopallium, nucleus

152   rotundus) are identified by the empty spaces between tracts. The population-based tractogram

153   provides a clear delineation of various brain regions and highlights the connections throughout the

154   brain. The applied fixel-based approach cannot report on the microstructure within different brain

155   nuclei; but rather sheds light on the fiber tracts surrounding and interconnecting them. As such, it

156   provides an excellent tool to investigate neuroplasticity of different brain networks without focusing

157   on changes within the nuclei, but still allowing defining them through their surrounding fibres,

158   referred to as HVC surr, RA surr and Area X surr.

159

160
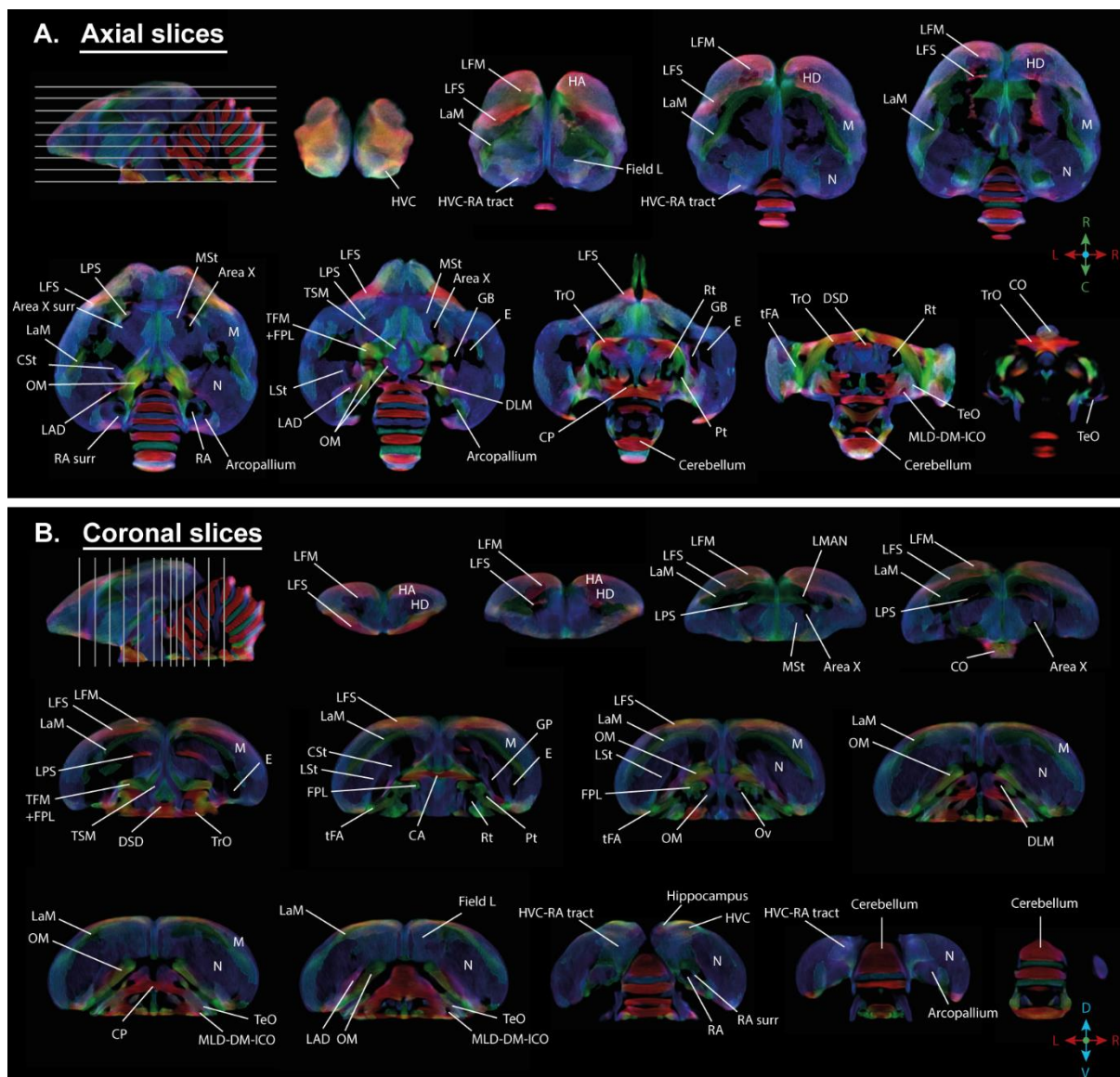
Figure 2. **Overview of the population based tractogram of male and female starlings over the seasons created for the fixel-based analysis with indications of different lamina, interconnecting tracts, nuclei and brain regions displayed on axial (A) and coronal slices (B) throughout the brain.** The different intervals of the coronal and axial sectioning are indicated on the saggittal inset in the left corner of each panel. The coronal slices do not follow a strict interval to visualise small nuclei such as DLM and Ov. The crosshair indicates the color-coding of the tractogram following the standard red-green-blue code (red = left-right orientation (L-R), blue = dorso-ventral (D-V) and green = rostro-caudal (R-C)). For abbreviations see abbreviation list.

3.2 DATA-DRIVEN ANALYSIS OF SEXUAL DIMORPHISMS IN BRAIN STRUCTURE

We established the general structural differences between male and female starling brains by applying a full-factorial design voxel-based analysis to our DTI data (figure 3, 4, Table 2). This includes data from all time points with time as a within-subject factor that needs to be averaged over (McFarquhar, 2019). This analysis confirmed the well-established sexual dimorphism of vocal control areas in songbirds (Bernard et al., 1993; Hamaide et al., 2017; Nottebohm and Arnold, 1976), where male starlings have higher FA in several parts of the song control system (the surroundings of HVC, Area X and RA) and auditory system (Field L and caudomedial nidopallium (NCM)) compared to female starlings. Interestingly, even though most differences occur bilaterally, these structures are visible as sub peaks within a single significant cluster. This cluster was asymmetric towards the left hemisphere and comprised large parts of the mesopallium and nidopallium, but not the lamina mesopallialis (LaM) which divides these regions. This means that not only the fibers surrounding the song control nuclei display different FA values, but also a larger part of the left hemisphere. In general, FA provides a correlate for a set of underlying microstructural characteristics related to structure and spatial organization of axons, dendrites and even cells, but cannot pinpoint a single underlying cellular event, as this requires dedicated histological studies (Sagi et al., 2012; Zatorre et al., 2012). Importantly, females generally have higher FA in tracts interconnecting both hemispheres (commisura anterior and posterior) and in bilateral tracts interconnecting nuclei within a hemisphere including the TrO, OM, septopallio-mesencephalic tract (TSM) and fronto-arcopallial tract (tFA). In addition, females have higher FA within the cerebellum and caudal part of the lateral striatum (CSt) compared to males. These findings are further confirmed by fixel-based analysis; as many of the sexual dimorphisms in FA match with the FD statistical analysis (figure 4 A, B). Certain subregions of the cerebellum, the molecular layer of cerebellar lobules II, III, IV have higher FD in females, whereas the cerebellar lobule VIII has higher FD in males. This diversifies the finding of increased FA in the cerebellum of female starlings. The molecular layer consists of parallel fibers emitted by the granule cells of the cerebellar cortex (D'Angelo, 2018). Fixel-based analysis is able to detect significant changes in this highly organized fibre structure, which is depicted as the red parallel fibers running left to right in figure 4 – figure supplement 1B. In addition to these microscopic changes, log FC statistical analysis revealed some macroscopic differences between male and female starlings (figure 4 C, D). Male starlings generally have a larger volume in the rostral part of the left hemisphere at the level of the hyperpallium apicale, which further supports the asymmetry towards the left hemisphere. Furthermore, the left HVC surroundings and cerebellar lobule VIII are larger in males compared to females. However, certain regions within the superior frontal lamina (LFS), nidopallium and mesopallium are larger in females, compared to males.

10

203 Alongside the well-established difference in the song control system, the applied data-driven
204 approach sheds new light on sexual dimorphisms in the rest of the starling brain, including a
205 microstructural hemispheric asymmetry towards the left hemisphere in males and a more structurally
206 organized cerebellum as well as several white matter tracts in females.

207
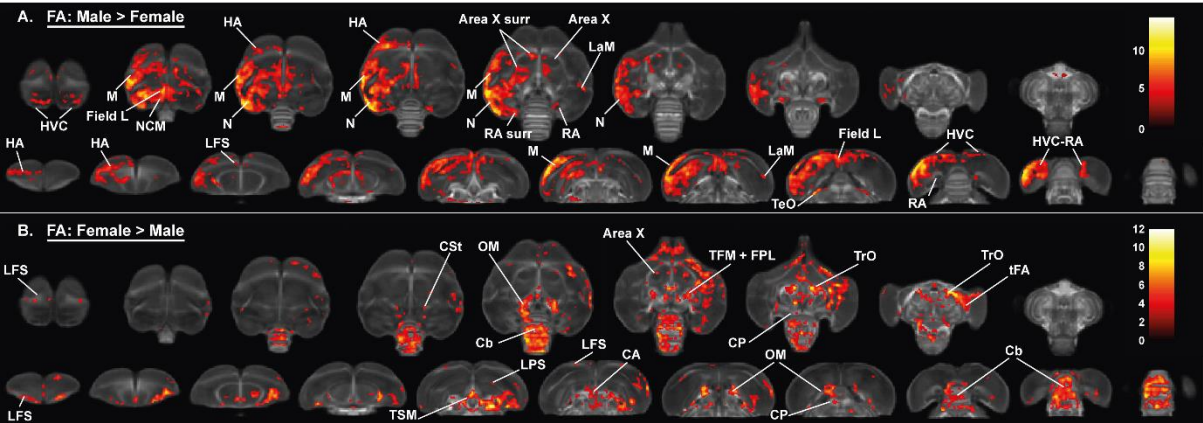
Figure 3: Overview of the general structural sexual dimorphism within the starling brain attributed to differences in fractional anisotropy (FA). For each sex comparison, the statistical parametric maps are displayed on axial and coronal sections throughout the brain (upper and lower row respectively). The results are displayed with $p_{uncorr} < 0.001$ and $k_E \geq 10$ voxels, and overlaid on the population FA map. The T-values are colour-coded according to the scale on the right. In males, FA was higher in a large cluster lateralized to the left hemisphere and covering parts of the nidopallium and mesopallium, including several regions of the auditory system and surrounding the song control system. Females, on the other hand, have higher FA at the level of the cerebellum and several tracts such as OM, TSM and TrO. For abbreviations see abbreviation list.

Table 2: Clusters displaying a sex difference in fractional anisotropy (FA)

Main sex difference for FA	Cluster	Hemisphere	Cluster		Peak	
			p_{FWE}	k_E	p_{FWE}	T
male > female	Nidopallium / mesopallium	Left	0.000	36936	0.000	14.25
	HVC surr	Left			0.000	8.35
		Right			0.000	7.53
	Field L dorsal	Left			0.000	10.00
		Right			0.000	6.93
	NCM	Left			0.000	7.72
		Right			0.000	6.72
	Area X caudal surr	Left			0.001	5.69
		Right			0.001	6.07
	RA surr	Left			0.000	7.86
	HVC-RA tract	Left			0.000	6.68
	RA surr	Right	0.000	441	0.001	6.08
	HVC-RA tract	Right			0.000	6.42

11

	TeO (superior)	Left	0.000	189	0.000	9.44
		Right	0.000	125	0.000	7.47
	LaM	Right	0.000	165	0.000	6.97
	Cerebellum	Lobule VII	0.011	101	0.000	6.54
female > male	TrO	Right	0.000	24846	0.000	12.08
		Left			0.000	8.84
	TSM	Left			0.000	9.62
		Right			0.000	9.74
	Commisura anterior	Center			0.222	4.85
	Commisura posterior	Center			0.066	5.19
	OM	Left			0.000	8.77
		Right			0.000	7.78
	CSt	Left			0.000	8.50
		Right			0.000	7.64
	Cerebellum	Lobule VIII			0.000	9.12
		Lobule VII			0.000	9.68
		Lobule VI			0.000	7.77
		Lobule V			0.000	7.12
		Lobule IV			0.000	6.58
	tFA	Right			0.000	10.50
		Left	0.006	113	0.000	8.64
	Area X	Left	0.139	57	0.000	6.34
		Right	0.000	254	0.000	6.91

218 Table summarizing the significance at cluster level and peak level. Some clusters are large and cover

219 multiple regions, indicated by the single statistic at cluster level. For each sub-region within this large

220 cluster the peak significance (pFWE) and T-value (T) are reported. P-values are FWE corrected. K_E

221 indicates the number of continuous voxels within a cluster. For abbreviations see abbreviation list.
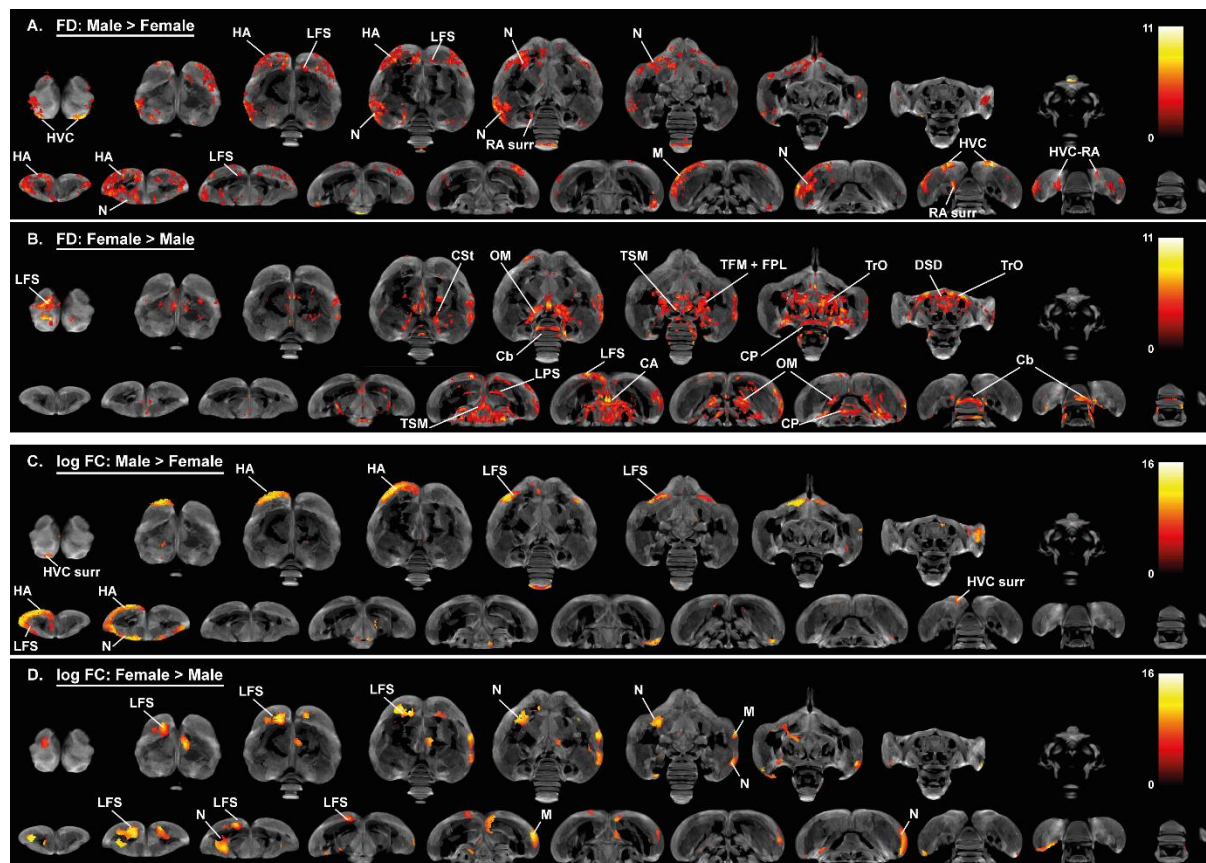
Figure 4: Overview of the general structural sexual dimorphism within the starling brain attributed to microscopic differences in fiber density (FD) (A, B) and macroscopic differences in fiber-bundle cross-section (log FC) (C, D). For each sex comparison, the statistical parametric maps are displayed on axial and coronal sections throughout the brain (upper and lower row respectively). The results are displayed with $p_{uncorr}<0.001$, and overlaid on the population based tractogram. Only significant tracks are displayed in a color representing the T-value. For abbreviations see abbreviation list.

229

Figure 4 – figure supplement 1: Overview of the general structural sexual dimorphism within the starling brain attributed to microscopic differences in fiber density (FD) (A, B) and macroscopic differences in fiber-bundle cross-section (log FC) (C, D) using fiber orientation color coding. For each sex comparison the statistical parametric maps are displayed on axial and coronal sections throughout the brain (upper and lower row respectively). The results are displayed with $p_{uncorr}<0.001$, and overlaid on the population based tractogram. Only significant tracks are displayed in a color according to the fiber orientation using the standard red-green-blue code as indicated by the crosshair (red = left-right orientation (L-R), blue = dorso-ventral (D-V) and green = rostro-caudal (R-C)). For abbreviations see abbreviation list.

3.3 ROLE OF BRAIN SIZE IN THE GENERAL SEXUAL DIMORPHISM

The hypothesis of neuronal interconnectivity is used to explain some of the sexual dimorphisms in brain structure of mammals and postulates that larger brains have relatively stronger intrahemispheric connections, resulting in stronger lateralization in larger brains, whereas smaller brains benefit more from higher interhemispheric connectivity (Hanggi et al., 2014). To ensure that the general sexual dimorphisms are attributed to a genuine sex difference and not to a difference in brain size, we examined: (1) whether there is a difference in brain size between males and females and; (2) if this difference in brain size can explain sexual dimorphisms like the higher interhemispheric

14

247 interconnectivity found in females. Even though there was a small difference in brain size between

248 male and female starlings (respectively, Mean male= 1815, SE= 8 mm³ and Mean female= 1770, SE=

249 13 mm³), it was not significant ($F_{(1, 23)}$=1.78, p=0.195). Next, we artificially divided each sex in two

250 groups based on their brain size using a median split similar to the analysis in Kurth et al. (2018)

251 (respectively, females: N=6 large and N=6 small, males N=6 large, N=7 small).

252 These artificially generated groups were used for a voxel-based analysis with brain size as a fixed factor

253 to assess the effect of brain size on the FA, FD and log FC analysis (figure 5, 6, figure 6- figure

254 supplement 1, table 5). This revealed that only a few sex differences could be attributed to a difference

255 in brain size. Large brain male and female starlings had higher FA values in specific sections of the

256 caudal surroundings of the right Area X, surroundings of RA and HVC compared to small brain male

257 and female starlings (figure 5A). The brain size difference in FA in right Area X surroundings and

258 cerebellum was matched with a difference in FD (figure 6A), whereas the higher FA in the surroundings

259 of HVC of large brain starlings, is complemented by a higher log FC in the surroundings of HVC (figure

260 6C).

261 Small brain starlings had higher FA in left NCM, a small part of the right LaM and TrO (figure 5A), which

262 closely matches the FD brain size difference in the left NCM and right LAM (figure 6B) and the log FC

263 difference in TrO (figure 6D). Following the hypothesis of neuronal interconnectivity, the voxel-based

264 statistical analysis for brain size is in line with the statistical analysis for sex at the level of the TrO, but

265 not in the NCM where both male and small brain starlings exhibit high FA. This might be partially

266 explained by the finding of higher log FC values in the NCM of large compared to small brain starlings

267 (figure 6C). Furthermore, some regions such as the hippocampus in large brain starlings and ventricle

268 in small brain birds were not detected in the voxel-based sex difference analysis and are solely

269 attributed to a difference in brain size. In the log FC analysis for brain size differences, more regions

270 unrelated to a sex difference showed a significant larger log FC value in large brains compared to

271 smaller brains, including parts of the pallial-subpallial lamina, lateral forebrain bundle, medial and

272 lateral surroundings of entopallium.

273 Interestingly, many of the fiber tracts that had a pronounced sex difference, such as the anterior and

274 posterior commissure, TSM and OM, were not found in the brain size statistical maps. Furthermore,

275 the microstructural hemispheric asymmetry covering the nidopallium and mesopallium detected in

276 the voxel-based sex difference analysis can also not be attributed to a mere difference in brain size.

277 Importantly, further statistical analysis is required to ensure that the brain size effect is not

278 confounded by other factors such as song behavior differences.

15

279 **Table 3: Clusters displaying a difference in brain size versus a difference in sex in fractional**

280 **anisotropy (FA)**

	Cluster	Hemisphere	Cluster		Peak		Relevant difference
			p_{FWE}	k_E	p_{FWE}	T	
Large> small brain	HVC surr	Left	0.000	227	0.000	6.43	M>F
	Hippocampus	Left	0.000	155	0.000	5.63	↑Singing F
	LaM/LFS	Left			0.000	7.51	
	HVC surr	Right	0.000	417	0.000	6.61	M>F
	Hippocampus	Right			0.000	6.94	
	Area X caudal surr	Right	0.000	190	0.002	5.99	M>F ↑Singing F
	LPS	Left	0.004	126	0.006	5.78	
	LPS/LFS	Right	0.000	337	0.042	5.29	
	tFA	Right	0.925	20	0.029	5.39	F>M
	TrO	Right	0.001	160	0.000	7.29	F>M
	RA surr	Left	0.000	451	0.193	4.88	M>F
	Cerebellum	Lobule VI			0.000	7.50	
	Cerebellum	Lobule VI	0.259	48	0.010	5.64	
	Cerebellum	Lobule IV	0.114	62	0.003	5.94	
	Cerebellum	Lobule VII	0.101	64	0.041	5.30	
Small > large brain	NCM	Left	0.006	116	0.000	6.39	M>F
	LaM	Right	0.014	100	0.025	5.43	
	Ventricle rostral	Left	0.217	51	0.000	7.21	
		Right	0.000	246	0.000	6.83	
	Ventricle caudal	Center	0.002	138	0.003	5.90	
		Center	0.004	122	0.214	4.84	
	TrO	Center	0.011	105	0.232	4.82	F>M

281 Table summarizing the significance at cluster level and peak level. Some clusters are large and cover

282 multiple regions, indicated by the single statistic at cluster level. For each sub-region within this large

283 cluster the peak significance (pFWE) and T-value (T) are reported. P-values are FWE corrected. K_E

284 indicates the number of continuous voxels within a cluster. The final column reports if a region with a

285 difference in brain size is analogue to other relevant differences such as the general sexual

286 dimorphism in FA (M>F or F>M) or the correlation between song rate and FA in females (↑Singing F).

287
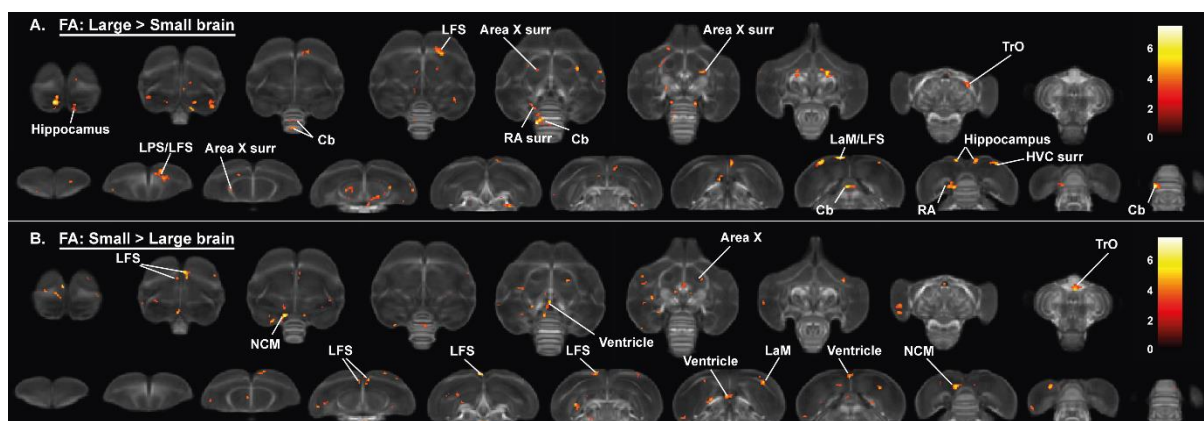
288 **Figure 5: Overview of general structural difference between large and small brain starling in**

289 **fractional anisotropy (FA).** The statistical parametric maps are displayed on axial and coronal sections

290 throughout the brain (upper and lower row respectively). The results are displayed with $p_{uncorr}<0.001$

291 and $k_E \geq 10$ voxels, and overlaid on the population FA map. The T-values are colour-coded according to

292 the scale on the right.

293
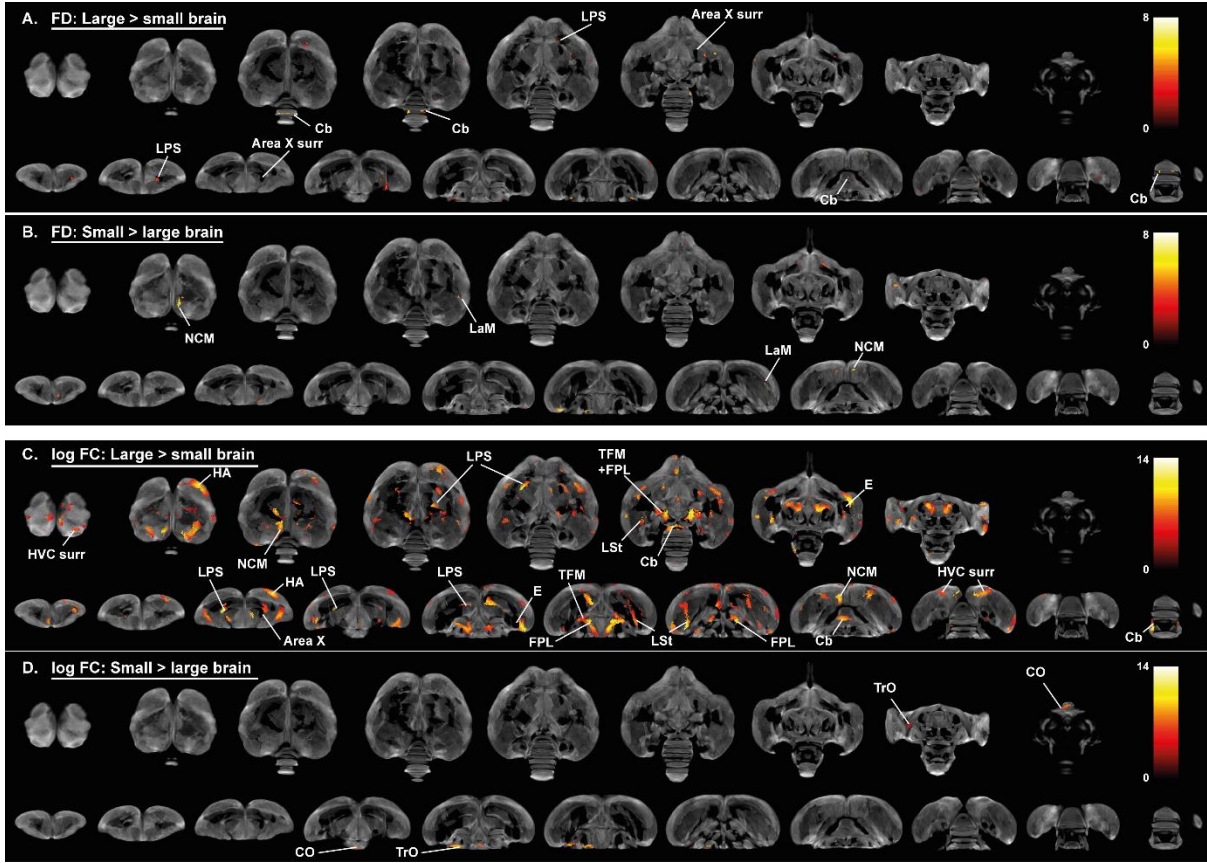
294 **Figure 6: Overview of general structural difference between large and small brain starling in**

295 **microscopic differences in fiber density (FD) (A, B) and macroscopic differences in fiber-bundle**

296 **cross-section (log FC) (C, D).** The statistical parametric maps are displayed on axial and coronal

297 sections throughout the brain (upper and lower row respectively). The results are displayed with

298 $p_{uncorr}<0.001$, and overlaid on the population-based tractogram. Only significant tracks are displayed

299 and colored according to their significance by T-value.

17
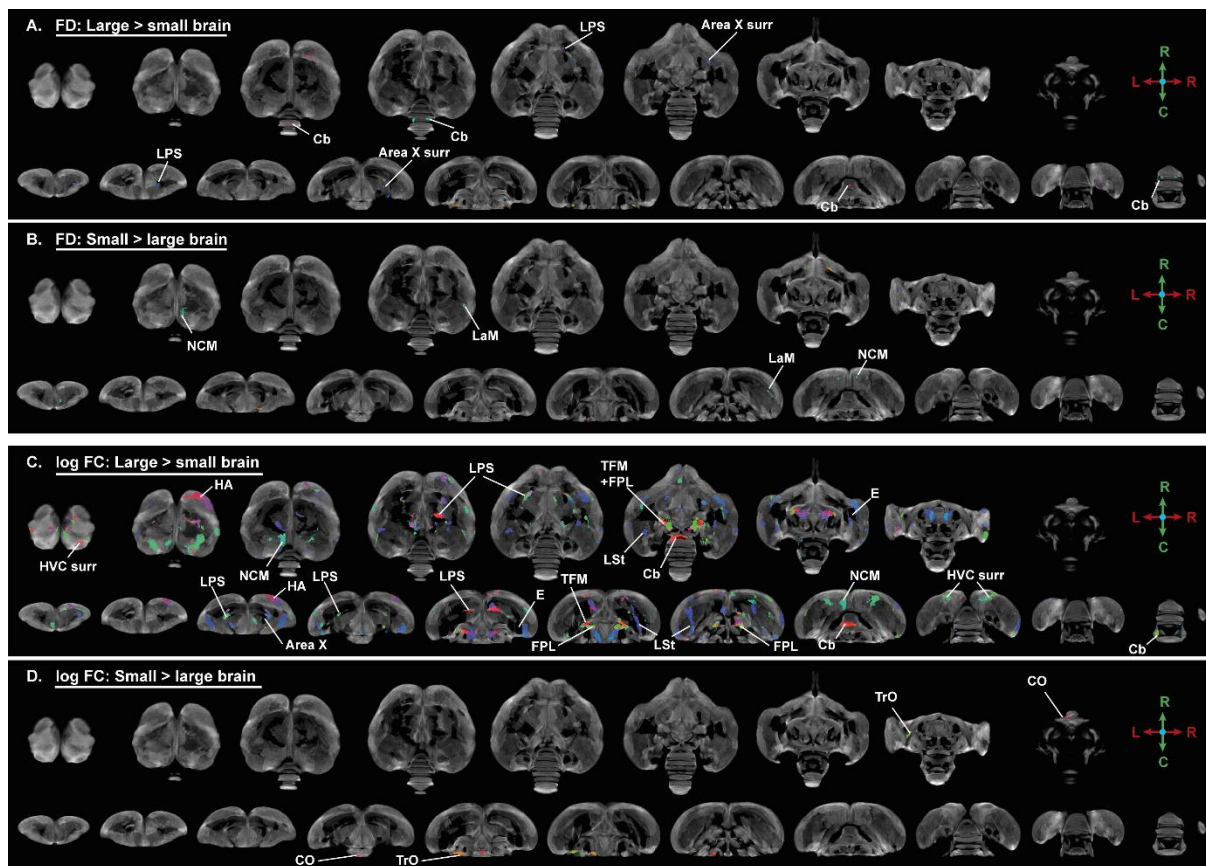
Figure 6- figure supplement 1: Overview of general structural difference between large and small brain starling in microscopic differences in fiber density (FD) and macroscopic differences in fiber-bundle cross-section (log FC) using fiber orientation color coding. The statistical parametric maps are displayed on axial and coronal sections throughout the brain (upper and lower row respectively). The results are displayed with $p_{uncorr}<0.001$, and overlaid on the population based tractogram. Only significant tracks are displayed and are colored according to the fiber orientation using the standard red-green-blue code as indicated by the crosshair (red = left-right orientation (L-R), blue = dorso-ventral (D-V) and green = rostro-caudal (R-C)). For abbreviations see abbreviation list.

3.4 SEXUAL DIMORPHISM IN SEASONAL NEUROPLASTICITY

After establishing the general structural sexual dimorphisms, we investigated whether seasonal neuroplasticity occurs differently between sexes. Therefore, we performed a voxel-based flexible factorial analysis looking at the general FA changes over time and the interactions between time and sex. These results are summarized in figure 7 and table 4. We extracted the mean FA values from the significant clusters and plotted them to determine how FA changes over time (figure 8). FA changes can be caused by a multitude of underlying microstructural changes, however FA is most sensitive to changes in axon number and density, axon diameter, myelination (see table 1). Additionally, we extracted the mean of the other diffusion parameters (MD, AD and RD) and fixel-based measures from these ROIs to provide more insight into the basis of the FA change (figure 8 - figure supplements 1-5). For the statistical analysis of the extracted parameters, we conducted a linear mixed model analysis with Tukey's Honest Significant Difference (HSD) multiple comparison correction during *post hoc* statistics.

3.4.1 Sexual dimorphism in seasonal neuroplasticity is lateralized and restricted to specific regions of the song control and auditory system

Voxel-based analysis picked up a significant interaction between sex and time in the surroundings of HVC (bilateral), in a rostro-lateral part of left RA surroundings and in left NCM (figure 7, 8). At the level of HVC surroundings and left NCM, males show a significant increase in FA during the photosensitive period at SD8 compared to photorefractory phases PR (left HVC $t(5, 54.7)= -4.09$, $p=0.0019$, right HVC $t(5, 55.0)= -3.09$, $p=0.0349$) and LD16 (left HVC $t(5, 54.7)= 3.66$, $p=0.0071$, right HVC $t(5, 55.0)= 3.71$, $p=0.0061$, left NCM $t(5, 54.3)= -3.71$, $p=0.0061$). In contrast, in females FA slightly decreases over time during the photosensitive and photostimulated phase. The change in FA in the male HVC surroundings is also reflected in other diffusion parameters (MD, AD, RD), but not in FD (figure 8 - figure supplement 1). Interestingly, the surroundings of left HVC were larger in males compared to females, as indicated by log FC sex difference ($F(1, 23.2)=13.9$, $p=0.0011$). The sex difference in FA in left NCM ($F(1, 21.6)=11.9$, $p=0.0024$) can be attributed to a sex difference in RD, where RD is lower in males compared to females ($F(1, 23.2)=109.2$, $p<0.0001$), suggesting a difference in myelin content or axon diameter (see table 1).

In the rostro-lateral surroundings of left RA, males and females do not differ from each other except on SD4 where males have significantly higher FA compared to the later time points; in contrast, females do not present any change over time in this specific part of RA surroundings. Even though there is no sex difference in FA, males do have lower AD and RD compared to females in this region (respectively, $F(1, 22.6)=39.6$, $p<0.0001$ and $F(1, 23.4)=60.3$, $p<0.0001$).

342   Whereas male FA increases significantly in specific parts of the surroundings of main song control

343   nuclei (HVC and left RA) and of the auditory system (left NCM), in females FA values remain constant

344   or even decrease over time. Male FA increase during the photosensitive period in NCM and HVC

345   surroundings is reflected in increased diffusion in all directions (MD, AD and RD all increase over time

346   (figure 8 – figure supplement 1).

347   ### 3.4.2   Similar seasonal neuroplasticity in both sexes mostly occurs in the photosensitive stage.

348   While some specific regions of the song control and auditory circuit present sexually dimorphic

349   neuroplasticity, most neuroplasticity occurs in parallel in males as in females; not only in regions

350   related to song control but also other sensory systems and the cerebellum (figure 7, 8). Within the

351   song control system, sexually analogous neuroplasticity occurs in the surroundings of right rostral

352   HVC, RA, Area X (rostral and caudal surroundings) and within left LMAN. More specifically the earliest

353   change was seen at four weeks of short days, in the caudal and rostral regions surrounding Area X. FA

354   values in Area X surroundings peaked around the end of the photosensitive period, sometimes

355   showing a slight dip at LD4 but generally remaining high even at LD16. The caudal part of left RA

356   surroundings presents increased FA values as early as 8 weeks of short days in both sexes, while in the

357   rostral surroundings of right HVC males increase FA at SD8 and females increase FA at SD12. In

358   contrast, the rostro-medial surroundings of right RA only shows a significant increase in FA at

359   photostimulation (male PR vs LD4 $t(5, 55.7)= -3.05$, $p=0.0386$, females PR vs LD4 $t(5, 54.0)= -4.91$,

360   $p=0.0001$). However, both in left and right RA surroundings, FA values remain elevated after sixteen

361   weeks of long days. In the right HVC rostral surroundings, FA remains high in the male starlings,

362   whereas females show a slight dip in FA during the photostimulated phase before increasing again

363   during the photorefractory phase (female LD4 vs LD16 $t(5, 53.9)= -3.74$, $p=0.0057$). The LMAN is one

364   of the last song control nuclei to change with increased FA levels at SD12 and LD4 relative to PR,

365   following a similar pattern in males and females.

366   In several song control nuclei, FA starts to increase early in the photosensitive period in both sexes at

367   a similar pace, and remains high during the photostimulated and photorefractory period. These FA

368   changes can be mostly attributed to an increase in AD over time particularly in males (figure 8-figure

369   supplement 2-3). Female starlings have a rapid decrease in RD during the photosensitive period in

370   right HVC and Area X surroundings, whereas males present no, or limited, changes in RD (figure 8-

371   figure supplement 2-3). This suggests that myelination plays a role in the neuroplasticity of females

372   during the photosensitive period, whereas males display more changes in axon number or axon

373   density.

374 In line with the voxel-based analysis for sex differences, only the left RA and Area X surroundings

375 present FA values that are higher in males compared to females. However, both left and right Area X

376 surroundings of males have lower diffusion in all directions (MD, AD and RD) compared to females,

377 suggesting a higher tissue density or fiber organization in males (figure 8-figure supplement 2). Both

378 left and right RA surroundings have lower RD in males compared to females, suggesting males have

379 more myelin content or smaller axon diameter. However, in the right RA surroundings, AD is also

380 significantly lower in males, suggesting a lower axon number or axon density. Interestingly, female

381 starlings have larger MD, AD and log FC within LMAN compared to male starlings. This is in line with

382 the fixel-based sex difference in log FC that encompasses parts of LFS in close proximity to LMAN.

383 Besides the song control system, many other regions including several white matter tracts and the

384 cerebellum changed over time as well. Some of these structures are involved in song behavior such as

385 the OM, LaM and CSt. OM conveys projections from the arcopallium, including connections from RA

386 to downstream regions (Reiner et al., 2004), whereas CSt holds projections going to the auditory

387 system (Vates et al., 1996). Females already show significant changes as early as four weeks of short

388 days in OM and CSt, whereas males only have significant FA change at SD4 in the left OM and at SD12

389 in the right OM. In males, FA values of OM peak at SD12 and slightly decrease during photostimulation

390 (SD12 vs LD4 left $t(5, 55.6)= 4.04$, $p=0.0022$, right $t(5, 56.1)= 4.09$, $p=0.0019$). In females the FA values

391 in OM remain high during photostimulation and only gradually decrease in the subsequent

392 photorefractory state in left OM (SD12 vs LD16 $t(5, 54.1)= 4.60$, $p=0.0004$). These changes over time

393 in FA are closely matched by the changes in FD. In line with the voxel-based sex differences, female

394 starlings have higher FA and FD in OM and CSt compared to male starlings (figure 8, figure 8 - figure

395 supplement 3). The CSt distinguishes itself from the other neuroplastic regions, as FA and FD keep on

396 gradually increasing over time, even when switching from the photostimulated to the photorefractory

397 phase.

398 LaM is the dividing lamina between the mesopallium and nidopallium and caries connections of HVC

399 to Area X and of LMAN to RA (Nottebohm et al., 1982). In the left LaM, FA increased significantly after

400 eight weeks of short days in both sexes (females PR vs SD8 ($t(5, 54.1)= -3.72$, $p=0.0061$), males PR vs

401 SD8 ($t(5, 55.5)= -2.99$, $p=0.0454$)). FA levels remained elevated until SD12 in males and until LD4 in

402 females, but did not reach baseline levels at LD16. FD in the LaM shows a similar increase during the

403 photosensitive period, especially in males. Conversely, the increase in FA in females is mostly

404 contributed to a decrease in RD during the photosensitive period.

405 In other white matter structures such as the TrO, TSM and tFA most neuroplasticity changes start

406 during the photosensitive phase, but are only significant around SD12. FA values in these tracts often

21

407   remain high during the photostimulated phase, and afterwards return to photorefractory state levels.

408   As the name indicates, the optic tract is involved in visual processing. TSM is also involved in the visual

409   pathway as it conveys projections from the wulst to sites within the brain stem (Reiner et al., 2004).

410   tFA holds projections of the trigeminal sensorimotor pathway between the basorostral nucleus (in the

411   rostral pallium) and arcopallium (Reiner et al., 2004; Wild and Farabaugh, 1996). Only in the right tFA

412   and TSM do FA levels remain high at LD16. The FD changes in TrO, TSM and left tFA closely match the

413   changes over time in FA and confirm the sex difference detected in the fixel-based analysis (figure 8 -

414   figure supplement 4).

415   Interestingly, cerebellar lobules VII-VIII, which are part of the oculomotor cerebellum, significantly

416   increase in FA by the end of the photosensitive period, peak in FA during the photostimulated phase

417   in both sexes (PR vs LD4 males $t(5, 54.4)=-6.32$, $p<0.0001$, PR vs LD4 females $t(5, 54.1)=-7.98$,

418     $p<0.0001$) and return to baseline values at LD16. Similarly to the surroundings of Area X and right

419   HVC, the FA changes over time in females coincide with a decrease in RD during the photosensitive

420   period, but increased AD values in males (figure 8 - figure supplement 4). Overall, neuroplasticity in

421   structures related to song and auditory processing starts early into the photosensitive period (SD4 and

422   SD8). Structures related to other sensory systems, such as the TrO, TSM, tFA and cerebellum, only

423   show significant increases by the end of the photosensitive phase (SD12) and often have decreased in

424   FA again by the next photorefractory phase. Even though the majority of these neuroplasticity changes

425   occur similarly in males and females, they sometimes differ in their approach. FA changes in males are

426   mostly due to changes in AD; however, females show changes in RD over time.

427
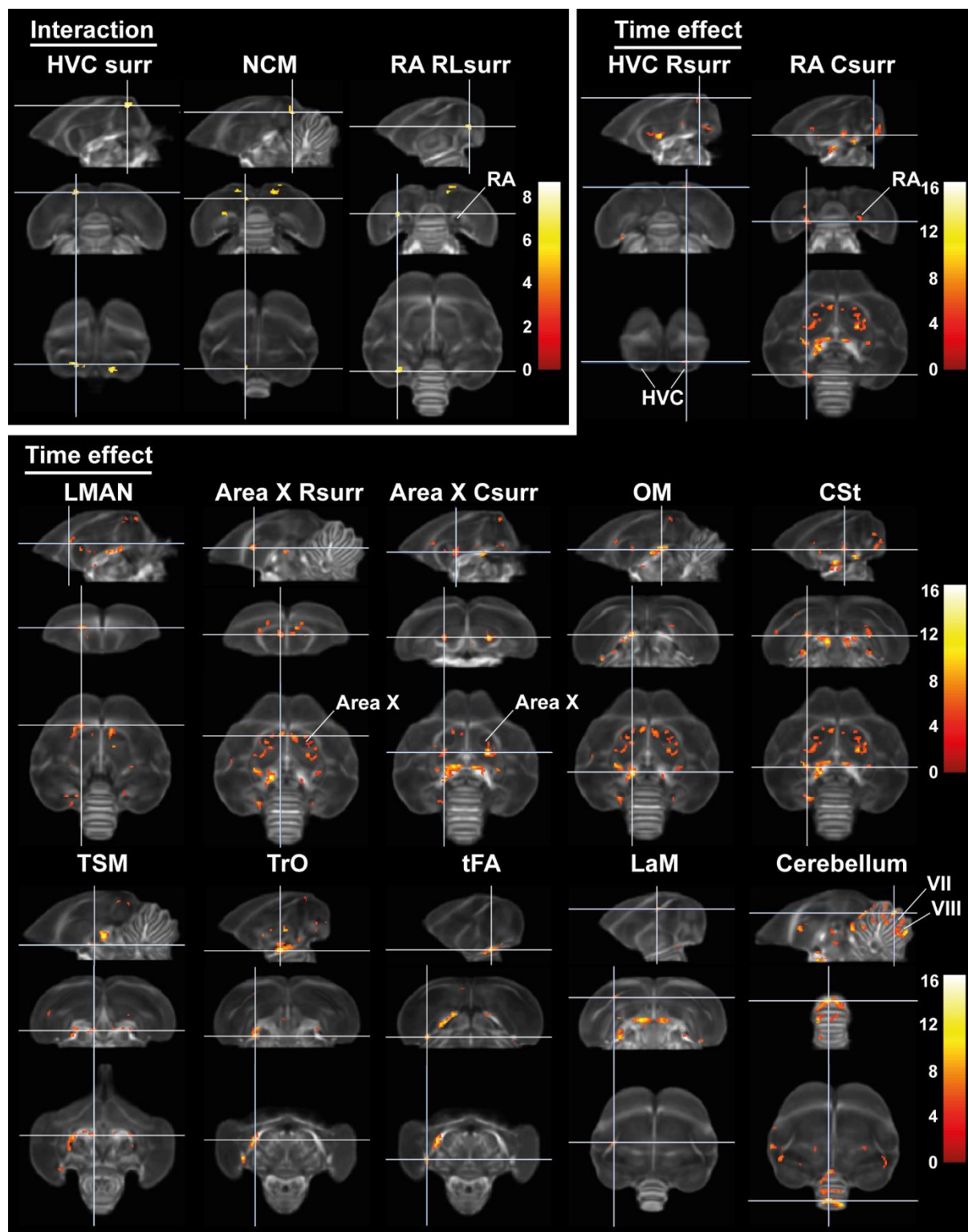
Figure 7: Time effect and interaction between sex and time in fractional anisotropy (FA) The statistical maps were assessed at $p_{uncorr}<0.001$ and $k_E \geq 10$ voxels with a small volume correction including regions of the white matter tracts, auditory and song control system. Main time effect of the cerebellum cluster was assessed without the small volume correction. Color scale represents significance by F-value. Abbreviations: C, caudal; RL, rostro-lateral; R, rostral; surr, surroundings.

Table 4: Clusters displaying a significant change over time and the interaction between sex and time in fractional anisotropy (FA)

Effect	Cluster	Hemisphere	Cluster		Peak	
			p_{FWE}	k_E	p_{FWE}	F
Interaction time * sex	HVC surr	Left	0.001	61	0.013	8.75
		Right	0.003	50	0.136	7.31
	RA rostro-lateral surr	Left	0.013	36	0.139	7.29
	NCM	Left	0.048	26	0.331	6.65
Main time effect	HVC rostral surr	Right	0.032	29	0.526	6.24
	RA caudal surr	Left	0.000	86	0.009	8.93
	RA rostro-medial surr	Right	0.006	42	0.017	8.57
	Area X caudal surr	Right	0.000	222	0.000	14.96
		Right	0.128	19	0.016	8.61
		Left	0.000	131	0.129	7.35
		Left	0.148	18	0.039	8.07
	Area X rostral surr	Left	0.000	76	0.007	9.09
		Left	0.037	28	0.144	7.27
		Right	0.000	176	0.000	11.05
	LMAN	Left	0.000	140	0.022	8.40
	OM	Left	0.000	513	0.000	16.44
		Right	0.000	158	0.002	9.75
	CSt	Left	0.000	82	0.003	9.53
		Right	0.001	61	0.048	7.95
		Right	0.025	31	0.242	6.89
	TSM	Right	0.009	39	0.009	8.97
		Left	0.001	56	0.074	7.70
	tFA	Left	0.000	91	0.000	12.73
		Right	0.015	35	0.042	8.03
	TrO	Left	0.000	302	0.000	14.18
		Right	0.001	58	0.264	6.83
	LaM	Left	0.037	28	0.120	7.40
	Cerebellum	Lobule VII	0.000	1779	0.000	15.26
		Lobule VIII			0.000	13.17

Table summarizing the significance at cluster level and peak level. Some clusters are large and cover multiple regions, indicated by the single statistic at cluster level. For each sub-region within this large cluster the peak significance (pFWE) and T-value (T) are reported. P-values are FWE corrected. K_E indicates the number of voxels within a cluster. Grey values indicate clusters that are significant at cluster level but not at peak level. Abbreviations: surr, surroundings

24
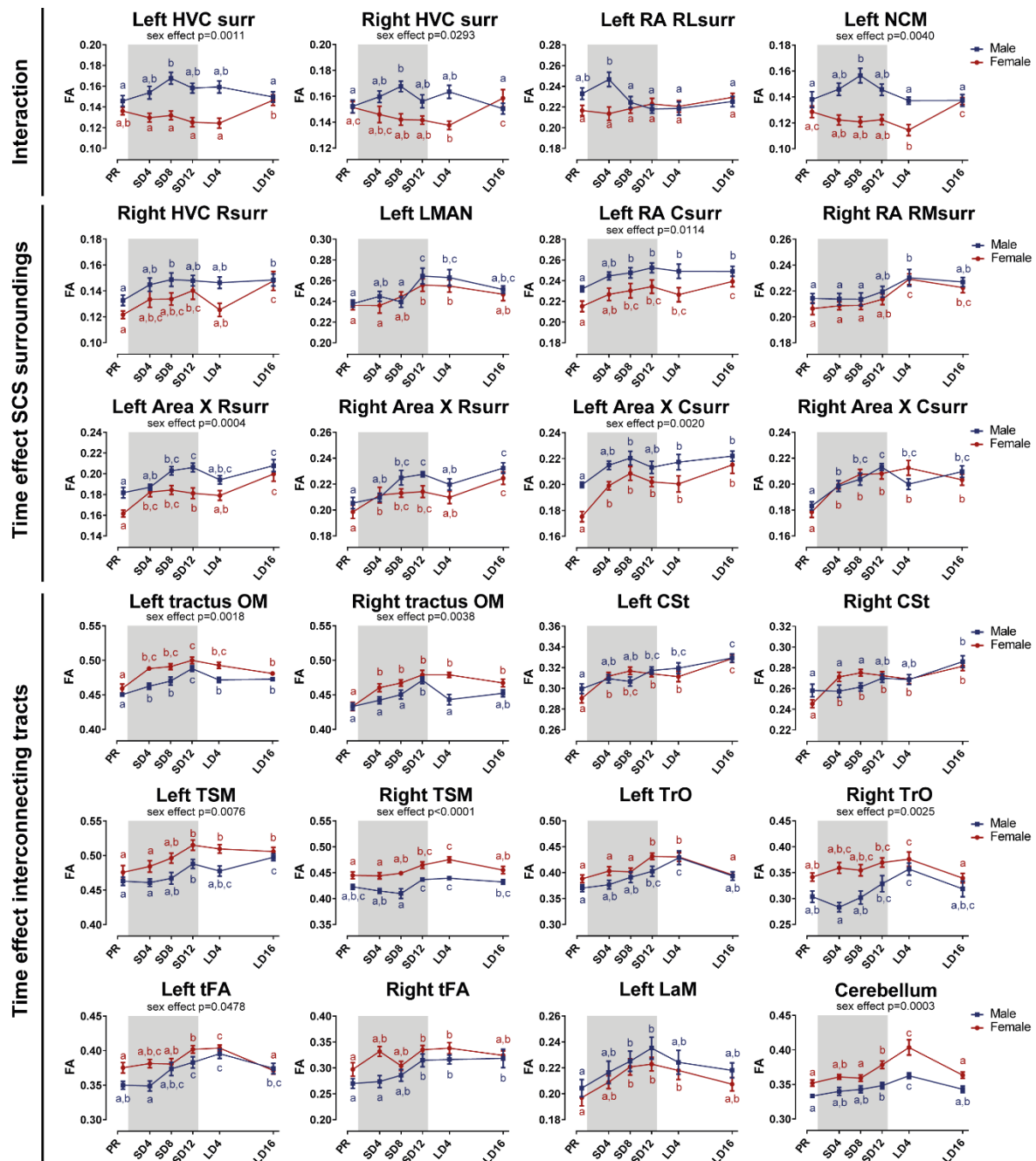
Figure 8: Summary of the longitudinal changes over time of FA extracted from ROI-based clusters that showed a significant interaction (first row), a significant change over time in the surroundings of song control nuclei (row 2 and 3) or a significant change over time in the fiber tracts (row 4 - 6). *The grey area indicates the entire photosensitive period of short days (8L:16D). Significant sex differences are reported with their p-value under the respective ROI-based cluster. Different letters denote significant differences by comparison with each other in post-hoc t-tests with p < 0.05 (Tukey's HSD correction for multiple comparisons) comparing the different time points to each other. If two time points share the same letter, the FA values are not significantly different from each other.* Abbreviations: C, caudal; RL, rostro-lateral; R, rostral; surr, surroundings.

3.5 PHOTOPERIODIC VARIATION IN HORMONE LEVELS AND SONG BEHAVIOR

In order to determine how the changes in neuroplasticity are related to changes in hormones and singing behavior across the different photoperiods, we collected blood samples and recorded songs at each time point. A linear mixed model analysis was performed to determine differences between sex, time and identify their interaction with HSD multiple comparison correction. This way, we validated whether the artificial photoperiod schedule induced hormonal changes comparable to the natural seasonal gonadal cycle in starlings.

3.5.1 Hormone levels

Plasma testosterone levels change significantly over time in both male and female starlings ($F_{(5, 98.0)}$=11.7, p<0.0001), but differed between sexes, as illustrated by a significant interaction ($F_{(5, 98.0)}$=4.82, p=0.0006) (figure 9A, B). In males, testosterone levels peak after four weeks of photostimulation (M= 1.67, SE=0.24) compared to photorefractory state PR (M= 0.03, SE= 0.26, $t_{(5, 43.8)}$=-4.73, p=0.0003). Two out of the thirteen male starlings already showed elevated plasma testosterone levels above 1ng/ml at the end of the photosensitive phase, but this increase was not significant at group level. In females, plasma testosterone levels are significantly elevated at the end of the photosensitive phase SD12 (M= 0.43, SE= 0.11) compared to LD16 (M= 0.01, SE= 0.10, $t_{(5, 54.2)}$=2.99, p=0.0461). Even though both sexes increase their circulating testosterone levels, female starlings do not reach the same levels as male starlings do.

Since testosterone is not the main reproductive hormone in female starlings, we also looked at changes in circulating estrogen levels (figure 9C). Similar to testosterone in males, plasma estrogen levels change significantly over time ($F_{(5, 48.3)}$=19.5, p<0.0001) with the highest concentrations measured after four weeks of photostimulation (M= 67.8, SE=3.26) compared to the photorefractory state PR (M= 47.7, SE=3.12 $t_{(48.3)}$=-4.88, p=0.0002). These increased circulating hormones at photostimulation confirm the reproductive maturation associated with the breeding season in starlings. Furthermore, we show that circulating testosterone levels already gradually increase during the photosensitive period in both sexes.
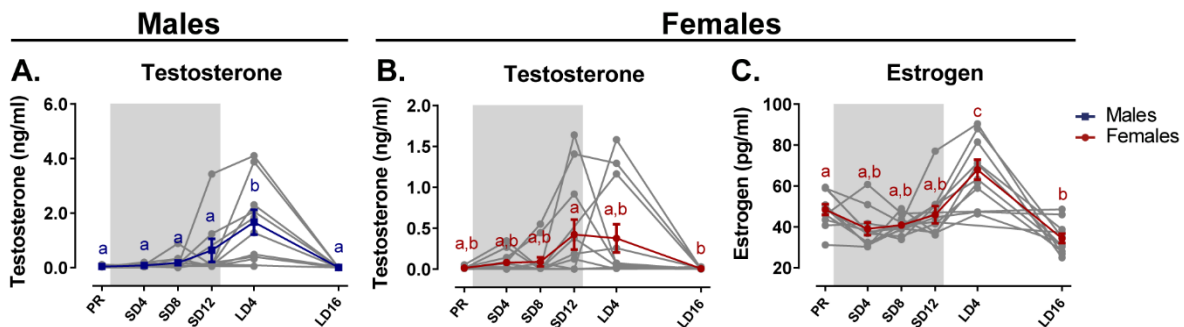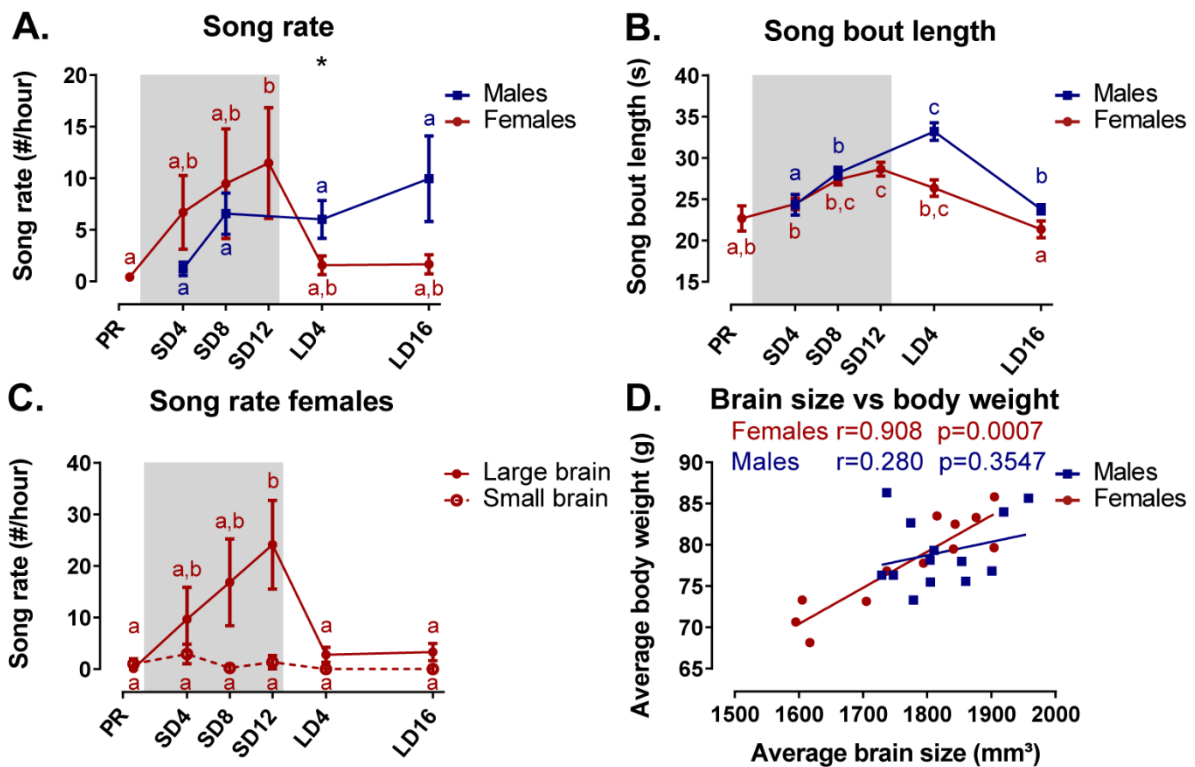
477 ***Figure 9**: **Overview of the seasonal changes in plasma testosterone (A, B) and estrogen (C)***
478 ***concentrations in male and female starlings.*** *Grey lines depict individual animals, while blue and red*
479 *lines represent the group average with the standard errors of the mean error bars. The grey area*
480 *indicates the photosensitive period of short days (8L:16D). Different letters denote significant*
481 *differences by comparison with each other in post-hoc t-tests with p < 0.05 (Tukey's HSD correction for*
482 *multiple comparisons) comparing the different time points to each other. If two time points share the*
483 *same letter, the testosterone level or estrogen level are not significantly different from each other.*

484 ### 3.5.2   Seasonal variation in song behavior and the role of brain size
485 Under artificial conditions, male starlings sing with a consistent song rate during every photoperiod.
486 In contrast, female starlings do show seasonal variation in song rate ($F_{(5, 42.1)}$=3.24, p=0.0145). They
487 sang most during the photosensitive phase (PR vs SD12 $t_{(5, 42.1)}$=-3.05, p=0.0428). During the
488 photostimulated phase, the song rate in females is drastically lower compared to males ($t_{(1,}$
489 $_{14.0)}$=5.39, p=0.0358) (figure 10A). In female starlings, the song bout length increased gradually over
490 time from (22.7 ± 1.5) s (M±SE) at the photorefractory phase to (28.6 ± 0.8) s at the end of the
491 photosensitive phase ($t_{(5, 336)}$=-2.97, p=0.0368), when their song rate and testosterone levels were
492 the highest (figure 10B). Male starlings presented a similar increase in song bout length over the
493 sequential photoperiods from (24.3 ±1.3) s at SD4 to (33.2 ± 1.1) s in the photostimulated phase
494 ($t_{(5,382.7)}$=-7.19, p<0.0001). Interestingly, song bout length was positively correlated at the within-
495 subject level to testosterone plasma levels in male starlings (rmcorr r=0.632, p=0.037). Such a
496 repeated measures correlation was not present in female starlings; neither did the song rate correlate
497 with testosterone levels in either sex.
498 We further investigated the effect of brain size on song behavior, using brain size (defined in result
499 section 3.3) as a fixed factor in the analysis of the song behavior for each sex separately. Interestingly,
500 the song rate of female starlings presented a significant effect of brain size and interaction between
501 brain size and time (respectively ($F_{(1, 10.8)}$ = 5.74, p=0.0358; $F_{(5, 37.6)}$= 3.14, p=0.0181). *Post hoc*
502 analysis quickly revealed that female starlings with a small brain rarely sing during any of the time
503 points (figure 10C). Large brain females were the most responsible in determining the seasonal change
504 in song rate and song bout length. Further analysis revealed that the brain size of the female birds is
505 proportional to their body weight, evident by positive Pearson's correlation between the averaged
506 brain size and averaged body weight (r=0.908 p<0.0001), which is not the case in the male starlings
507 (figure 10D). Female starlings with a large brain have a higher body weight and are capable of singing
508 with a high song rate during the photosensitive period unlike their smaller female counterparts.
509 Importantly, the interpretation of the sexual dimorphisms attributed to brain size is further

complicated, since the difference between large and small brain female starlings is confounded by their difference in singing behavior.


Figure 10: *Overview of the seasonal changes in song rate (A) and song bout length (B) in male and female starlings. Dividing the starlings based on brain size showed that only large brain female starlings sing (C). Females present a significant correlation between the average brain size and body weight (D).* (A-C) Blue and red lines represent the group average with the standard errors of the mean error bars. The grey area indicates the photosensitive period of short days (8L:16D). Different letters denote significant differences by comparison with each other in post-hoc t-tests with p < 0.05 (Tukey's HSD correction for multiple comparisons) comparing the different time points to each other. If two time points share the same letter, the song rate or song bout length are not significantly different from each other. (D) The Pearson's correlation and its significance are reported for males and females.

3.6 NEURAL CORRELATES OF SONG BEHAVIOR

Having established the seasonal changes in neuroplasticity and song behavior, we performed a voxel-based multiple regression analysis to determine the neural correlate of song behavior. Neither song bout length nor the male song rate presented a significant voxel-based correlation. However, female song rate correlated positively to FA in the left hippocampus and the surrounding fibers of RA and Area X (figure 11, Table 5). This correlation was not only linked to the overall difference between singing and non-singing females, but also to the increase of song rate within a subject as evidenced by the significant repeated measures correlation with FA of the caudal surroundings of Area X and left

28

530   hippocampus. Thus, we conclude that not only are large female starlings capable of producing more

531   songs, this increased song rate is also correlated to improved microstructural organization of some

532   major song control nuclei and the hippocampus.

533
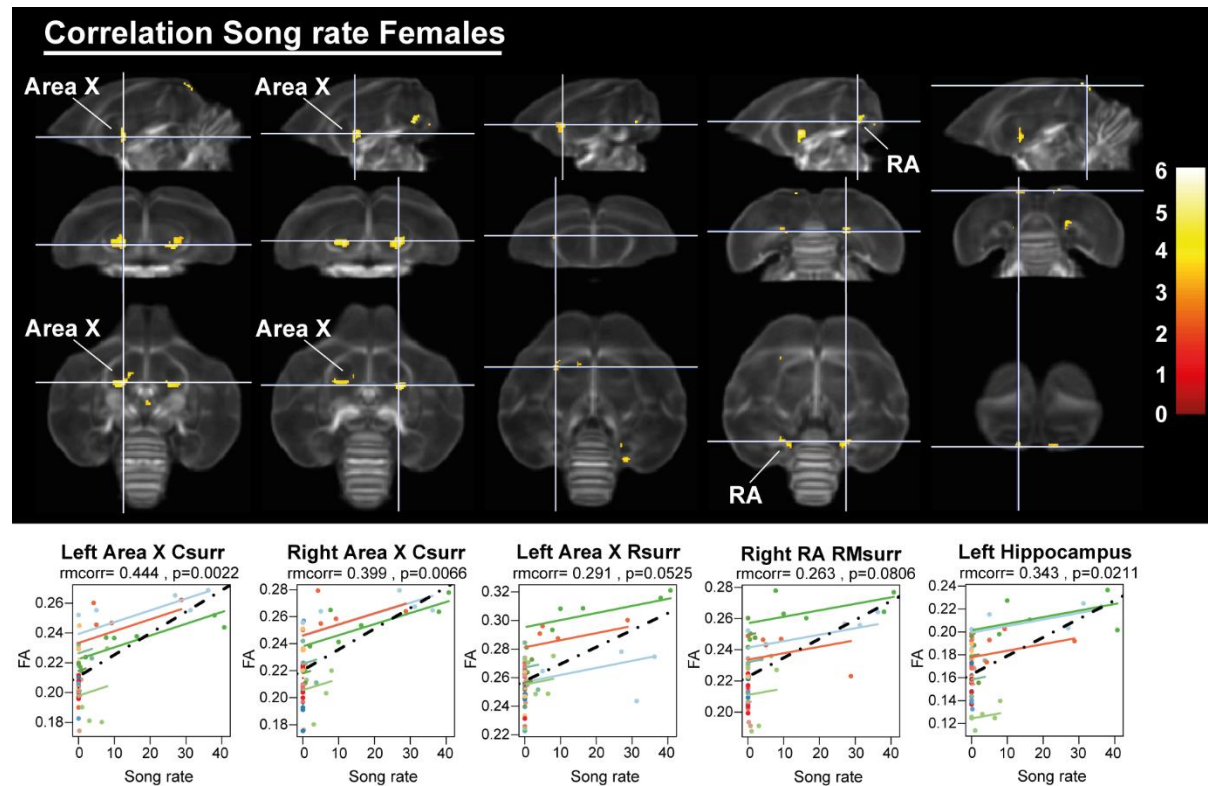
534   ***Figure 11: Overview of structural neural correlates of song rate to FA in female starlings.*** The

535   statistical maps were assessed at $p_{uncorr}<0.001$ and $k_E \geq 10$ voxels with a small volume correction

536   including regions of the song control system and other white matter structures. Below each statistical

537   parametric map, the identified correlations were further explored with repeated measures

538   correlation. Solid colored lines show the best linear fit for the within-subject correlation using parallel

539   regression lines for individual animals. The dashed line represents the linear fit of the overall Pearson

540   correlation representing the between-subject correlations. Abbreviations: C, caudal; RM, rostro-

541   medial; R, rostral; surr, surroundings.

542   **Table 5: Summary of the voxel-based correlation analysis of song rate vs FA in female starlings.**

Cluster	Hemisphere	Cluster		Peak		Pearson's correlation	Rmcorr	
		p_{FWE}	k_E	p_{FWE}	T	r	r	P
Area X caudal surr	Left	0.000	168	0.002	6.05	0.5396	**0.444**	**0.0023**
	Right	0.001	116	0.015	5.45	0.5045	**0.399**	**0.0066**
Area X rostral surr	Left	0.041	45	0.427	4.24	0.4587	0.291	0.0525
RA rostro-medial surr	Right	0.015	59	0.039	5.13	0.3969	0.263	0.0806
Hippocampus	Left	0.132	30	0.029	5.22	0.3883	**0.343**	**0.0211**

29

543 This table summarizes for each significant cluster-based ROI the voxel-based FWE corrected p-value

544 at cluster and peak level, next to the overall Pearson's correlation, the repeated measures correlation

545 (rmcorr) and its significance of the averaged FA values versus the respective song characteristic. K_E

546 indicates the cluster size. T reflects the t-value of the maximal peak located within the cluster-based

547 ROI. Voxel-based correlations in grey are significant at the cluster level, but not at peak level.

548 Significant repeated measures correlations are indicated in bold. Abbreviations: surr, surroundings.

4 DISCUSSION

550 The present data-driven longitudinal study confirms the well-established sexual dimorphism of the

551 songbird brain, showing that male starlings generally have a more structured song control system

552 compared to female starlings- as is the case in zebra finches where only the male sings (Hamaide et

553 al., 2017). We also demonstrated new ones, including the finding that females have stronger tracts

554 interconnecting hemispheres and nuclei, while males have a microstructural asymmetry towards the

555 left hemisphere. Interestingly, brain size does not completely explain the sexually dimorphic

556 hemispheric asymmetry of males or increased interconnectivity of female brains; only some of the sex

557 differences in certain song control nuclei could be attributed to brain size. However, the difference in

558 brain size is confounded by the difference in singing behavior of female starlings. Female starlings with

559 small brains rarely sing during any of the time points. In contrast, females with large brains are capable

560 of singing at a high song rate and strengthen their song control network during the photosensitive

561 period. In general, both male and female starlings display similar structural neuroplasticity not only in

562 the surrounding fibers of the song control system, but also in tracts related to other sensory systems

563 such as the auditory and visual network. Even specific parts of the cerebellum, related to the

564 processing of sensory information, display seasonal neuroplasticity. However, males and females

565 show slight differences in the way neuroplasticity is displayed. Male starlings, for example,

566 demonstrated significant neuroplasticity in HVC surroundings and left NCM, which was absent in

567 female starlings. Importantly, most of these neuroplasticity changes already start during the

568 photosensitive period, when circulating testosterone levels are low but gradually begin to increase in

569 both sexes.

4.1 GENERAL SEXUAL DIMORPHISM IN THE STARLING BRAIN'S TRACTOGRAPHY

571 *In vivo* DTI and fixel-based analysis, although focusing on fibers surrounding and interconnecting the

572 nuclear brain regions in the songbird brain, could capture the well-established structural sexual

573 dimorphism at the level of the song control system in songbirds (Bernard et al., 1993; Hamaide et al.,

574 2017; Nottebohm and Arnold, 1976). Even though the sexual dimorphism in the song control system

575   is bilateral, we demonstrated a strong asymmetry towards the left hemisphere in male starlings

576   covering the left nidopallium and mesopallium. Furthermore, analysis of seasonal neuroplasticity

577   confirmed this lateralization, as many clusters found in the left hemisphere (i.e. surroundings of left

578   HVC, RA, rostral and caudal surroundings of Area X) had higher FA values in males compared to

579   females. However, in many of the surroundings of song control nuclei, males had lower RD compared

580   to females, which implies that males have smaller axonal diameters or more myelinated fibers in these

581   structures (Song et al., 2005). In the rostral and caudal surroundings of Area X, diffusion in all

582   directions (MD, AD and RD) is larger in females compared to males, which suggests that females have

583   a less structured fiber organization or tissue density in this region (Beaulieu, 2002; Zatorre et al., 2012).

584   These observations might guide histological studies to shed more light on the underlying structural

585   differences causing these differences in FA. Left-right differences are not always examined in

586   histological studies. Most of the studies concerning hemispheric asymmetry or lateralization focus on

587   the lateralization of functions involved in the processing of auditory, visual and olfactory information

588   (Rogers, 2012). Often these studies use electrophysiology or functional MRI (fMRI) to quantify the

589   neural response to certain stimuli (De Groof et al., 2017; Yang and Vicario, 2015). Following the

590   Hebbian hypothesis (neurons that fire together, wire together), a lateralized firing pattern suggests

591   lateralized structural microstructure. Human imaging studies have combined fMRI and tract-tracings,

592   and found that white matter asymmetries may be one of the factors underlying functional

593   hemispheric asymmetries (Ocklenburg et al., 2013). Our study contributes to this hypothesis, showing

594   a large microstructural hemispheric asymmetry of the male starling brain, which might be underlying

595   some of the functional hemispheric asymmetries in starlings. Furthermore, this lateralization might

596   be species-specific; zebra finches by contrast exhibit no left-right difference in the volume of song

597   control nuclei (Nixdorf-Bergweiler, 1996). Prior DTI studies in zebra finches also did not find a sex

598   difference in cerebral asymmetry of song control nuclei (Hamaide et al., 2017).

599   Unexpectedly, females have higher FA in several tracts interconnecting nuclei of the visual and song

600   control system and in interhemispheric connections such as the commissure anterior and posterior.

601   This is in contrast to zebra finches where males have a larger white matter volume compartment

602   compared to females (Hamaide et al., 2018a). However, stronger interhemispheric connectivity is

603   present in female mammals, though this has been attributed to brain size rather than a real effect of

604   sex (Hanggi et al., 2014). Even though male starlings had a slightly -but not significantly- larger brain

605   compared to females, matching our findings in zebra finches (Hamaide et al., 2018a), our study could

606   not confirm the hypothesis of neuronal interconnectivity (Hanggi et al., 2014). The voxel-based

607   analysis for brain size could not explain the hemispheric asymmetry in males or the increased

608   interhemispheric connections in females. Brain size could only explain some sexual dimorphisms in

609 specific parts of the song control system, such as the caudal surroundings of the right Area X,

610 surroundings of RA and HVC. However, in females the difference in brain size is confounded by the

611 difference in song behavior. Our data reveal that female starlings with a large brain sing more,

612 especially during the photosensitive phase, compared to female starlings with a relatively smaller

613 brain. Furthermore, female song rate is correlated to FA in the same song control regions, e.g. the

614 surroundings of Area X and RA. Brain size is affected by multiple factors including age, circulating

615 hormone levels, environment and experience (Healy and Rowe, 2007). Of note, because we used wild

616 caught starlings we cannot control for their exact age or developmental history. The larger females

617 could be older compared to the smaller female starlings. In summation, these confounding factors

618 make it unlikely that the brain size difference is the sole explanation for the sexual dimorphisms.

619 Sexual structural dimorphisms of the brain might also be explained by sexual differences in behavior.

620 Take, for example, the sexual dimorphism of the TrO and TSM that carries projections to the wulst

621 (Reiner et al., 2004). Enhancement of the visual system in females could be related to the visual cues

622 like ultraviolet plumage colors female starlings take into consideration during mate selection (Bennett

623 et al., 1997). Moreover, this role of the visual system during the breeding season is further

624 corroborated by the neuroplasticity changes in the visual system, which occur at the end of the

625 photosensitive period, right before the onset of the photostimulated period and return to baseline

626 levels after sixteen weeks of long days. This is consistent with a prior DTI study, where the optic chiasm

627 of male starlings had lower FA values during the photorefractory state compared to the breeding

628 season (De Groof et al., 2008).

629 Interestingly, because of the limited research in the cerebellum of songbirds, we are the first to report

630 clear sexual dimorphisms in the fiber characteristics of specific lobules of the cerebellum. Females had

631 higher FA values in a large part of the cerebellum covering both anterior and posterior lobules IV-VIII,

632 and higher FD in anterior lobules II-IV. In males, mostly the posterior lobule VII had higher FA, whilst

633 lobule VIII had higher FD and log FC. The avian cerebellum has a strict topographic organization where

634 each cerebellar lobule has a distinct input and output (Arends and Zeigler, 1991). Anterior lobules (I-

635 V) contain the somatotopic representation of the tail, leg and wings (Whitlock, 1952) and are more

636 pronounced in avian species with strong hind limbs (Iwaniuk et al., 2007). Cerebellar lobules VII and

637 VIII are part of the oculomotor cerebellum (VI-VIII) and receive visual input (Clarke, 1977), input from

638 the pretecto-ponto-cerebellar system involved in flight (Wylie et al., 2018) and have a somatotopic

639 representation of the cochlea and retina (Whitlock, 1952). The pronouncement of the oculomotor

640 cerebellum in males versus females could reflect the integration of visual and auditory sensory input,

641 including the more developed song behavior of males. Language tasks in humans mostly involve the

642 lateral lobules VI and crus I/II, which are implicated in initiating the motor sequence of phonological

32

643 content, whereas VIIb/VIII support the phonological storage during the maintenance of verbal
644 information (Marien et al., 2014). However, there is only limited information on the specific cerebellar
645 lobules implicated in song production of songbirds. Recently a cerebello-thalamic-basal ganglia
646 pathway was identified that influences song processing, where lateral cerebellar nucleus (CbL)
647 projects to dorsal thalamic regions and coincides with retrograde label of Area X and medial striatum
648 (Person et al., 2008; Pidoux et al., 2018). Furthermore, lesioning Area X caused structural remodelling
649 within the cerebello-thalamo-basal ganglia pathway including the dorsal thalamic zone, CbL and
650 extended further in cerebellar lobules VIb and VII (Hamaide et al., 2018b). These lesions independently
651 affected the duration of syllables (Hamaide et al., 2018b; Pidoux et al., 2018), which indicates the
652 importance of the cerebello-thalamo-basal ganglia pathway in the timing of birdsong (Konopka and
653 Roberts, 2016). The cerebellum generally works as a forward controller, where it compares intention
654 with execution and uses the error information to correct future events (D'Angelo, 2018; Strick et al.,
655 2009). This conceptualization of the cerebellum as a learning machine was developed as a model for
656 motor control (Miall and Reckess, 2002), but can also be applied in other learning behaviors, such as
657 vocal learning in birds, since the forward control process of the cerebellum is especially implicated in
658 the timing of combined stimuli. Moreover, the oculomotor cerebellum exhibits neuroplasticity with a
659 similar temporal profile to the multisensory neuroplasticity observed in the cerebrum. The molecular
660 layer of the cerebellum contains the parallel fibers emitted by the granule cells and is known to
661 maintain a high level of neuroplasticity throughout life (Ito, 2006; Medina et al., 2002). Furthermore,
662 steroids can affect cerebellar Purkinje firing related to locomotor activity (Dean and McCarthy, 2008;
663 Smith, 1995). Together, these findings imply that the plasticity in song control system is not limited to
664 the known song circuitry but also involves the cerebellum.

665 The general sexual dimorphism in the starling brain extends well beyond the song control system, and
666 whilst for mammals this was suggested to be related to the difference in brain size, we do not find
667 evidence for that in avian species. The few sex differences in the song control system that could be
668 attributed to brain size are confounded by song behavior. Furthermore, many of the other sexual
669 dimorphisms involving the visual system and cerebellum could be explained by behavioral differences
670 between sexes. It can thus be reasonably assumed that the general structural sexual dimorphisms in
671 starlings are related to differences in behavior rather than brain size.

4.2 SEASONAL VARIATION IN GONADAL HORMONES, SONG BEHAVIOR AND ITS NEURAL CORRELATES

674 The seasonal variation in hormone levels (Dawson, 1983; Riters et al., 2002; Williams et al., 2004) and
675 song behavior during artificial photoperiod switching is in good agreement with the seasonal changes

33

676 observed in natural conditions. In male starlings on a natural cycle, hypothalamic GnRH expression is
677 already high in February under short days, which coincides with the start of the testes growth and
678 results in a gradual increase of circulating testosterone (Bentley et al., 2013; Dawson, 1983). Female
679 birds also produce testosterone, mainly in the ovaries and the adrenal gland (Tanabe et al., 1979).
680 Circulating testosterone levels are high in female starlings in the pre-laying phase and decrease after
681 ovulation, whereas estrogens are high during the breeding season in March and peak around ovulation
682 (Dawson, 1983; Williams et al., 2004). It is well known that estrogens are fundamental in the
683 regulation of female reproduction, whereas the role of testosterone in female reproduction is less
684 studied. However, female starlings are the most aggressive during the pre-laying period, when their
685 testosterone levels are high (Williams et al., 2004). Our study confirms that both male and females
686 present a gradual increase in circulating testosterone during the photosensitive phase. In males, this
687 was shown to coincide with an increase in hypothalamic GnRH expression (Bentley et al., 2013).
688 Furthermore, the current study showed that in male's testosterone plasma levels were positively
689 correlated to the song bout length on a within-subject level. We suggest that beside the effect of
690 testosterone on reproductive functions, it could also be important in the regulation of neuroplasticity
691 observed during the photosensitive phase.

692 ## 4.3 MALE AND FEMALE STARLINGS BOTH EXPERIENCE NEUROPLASTICITY IN THEIR SONG CONTROL
693 SYSTEM, BUT DIFFER IN THEIR SONG BEHAVIOR AND THE UNDERLYING MECHANISMS

694 Although structural neuroplasticity of the song control system is broadly similar in males and females,
695 there are some notable differences. We revealed that seasonal neuroplasticity differs between males
696 and females in specific parts of the HVC surroundings and left NCM, where only males experienced
697 seasonal neuroplasticity. Females by contrast only showed an FA increase in the more rostral part of
698 the right HVC surroundings after twelve weeks of short days. During photostimulation, when the
699 female singing behavior is lower, FA values in the right HVC surroundings dropped slightly.

700 After four weeks of short days, our earliest time point of the photosensitive period, females presented
701 a significant FA change in the OM, rostral and caudal Area X surroundings and the CSt, whereas males
702 only had significant FA changes in the left OM, left RA surroundings (interaction cluster) and caudal
703 surroundings of right Area X at that time point. Most of the neuroplasticity of song control nuclei like
704 HVC and Area X surroundings in males occurred only after eight weeks of short days. It seems as if the
705 song-related seasonal neuroplasticity occurs slightly sooner in females compared to males, especially
706 in the rostral surroundings of Area X, which is a part of the anterior forebrain pathway, and the CSt,
707 which is an auditory region. Both structures could play a role in the auditory feedback loop that is
708 associated with vocal learning (Bosíková et al., 2010). The female singing behavior was most

709   prominent during the photosensitive period in our experiment, which is in good agreement with

710   Pavlova et al. (2007). In contrast, males do not change their song rate over different photoperiods, in

711   agreement with Adret-Hausberger (1994), but do show seasonal variation in their song bout length,

712   in line with Van Hout et al. (2009). Sexual dimorphism at the level of the song control system suggests

713   that male circuitry already has a stronger microstructural organization compared to the females. Male

714   neuroplasticity changes in FA are mostly attributed to changes in AD, sensitive to changes in axon

715   number or axon density. Female starlings conversely demonstrated decreased RD during the

716   photosensitive period, indicating changes in myelin content or axon diameter, which was minimal in

717   males.

718   Furthermore, FA values in the Area X surroundings and hippocampus were positively correlated to the

719   female song rate on a within-subject level. The role of hippocampus in song behavior is not widely

720   understood. Previous work has mainly focused on the role of the hippocampus in spatial memory

721   performance (Macphail, 2002). Prior studies demonstrated that males generally outperform females

722   in spatial memory performance tasks, but rely on different strategies in learning such cognitive tasks

723   in both mammals and songbirds (Kosarussavadi et al., 2017; Rensel et al., 2015; Tropp and Markus,

724   2001). Sexually different learning mechanisms have also been suggested in vocal learning in songbirds

725   (Riebel, 2016). Few studies have looked at the role of the hippocampus in song behavior in zebra

726   finches. Hippocampal lesions during song learning and adulthood in male zebra finches did not affect

727   song learning, singing or song structure. However, in females, hippocampal lesions affected

728   preference for their father's song (Bailey et al., 2009). Interestingly, the hippocampus has a high

729   aromatase expression and is a site of immediate early gene expression in response to conspecific zebra

730   finch song, predominantly in female zebra finches (Bailey and Saldanha, 2015; Bailey and Wade, 2003;

731   Gobes et al., 2009). These findings suggest that the hippocampus might play a role in specific

732   characteristics of song perception, like identity and temporal context. To our knowledge, we are the

733   first to report on a potential role of the hippocampus in the song behavior of female starlings.

734   Interestingly, many of the seasonal changes in brain structures related to the singing behavior do not

735   return to baseline levels after sixteen weeks of long days. In males, the surroundings of HVC, left RA

736   and left NCM were not different between the two sample points in the photorefractory phases in our

737   study. Some structures such as the left OM show a gradual decrease in FA values at LD16 compared

738   to their peak at SD12. A potential explanation is that these singing related structures require more

739   time to return to baseline levels. Alternatively, certain regions related to song behavior may never

740   fully regress to baseline photorefractory levels, but instead increase year after year. Bernard et al.

741   (1996) demonstrated that in yearling starlings, HVC and RA volume was lower compared to older adult

742   starlings, which was linked to the increasing song repertoire of starlings over the years. Furthermore,

743 CSt related to the auditory system distinguishes itself from other structures as it keeps on increasing
744 in FA over subsequent photoperiods. This could represent a maturation upon aging, independent of
745 the seasonal changes.

746 Together these findings suggest that males and females, just like in spatial memory, use different
747 learning strategies in vocal learning as suggested by Riebel (2016). They rely on different parts of the
748 song control system and use different mechanisms to manifest neuroplasticity in their respective song
749 control system. Female starlings relied particularly on the auditory feedback loop and show
750 involvement of the hippocampus. Males, on the other hand, display greater utilization of the NCM,
751 left RA and HVC surroundings in their song control related neuroplasticity.

752 ### 4.4 THE PHOTOSENSITIVE PHASE IS A SENSITIVE WINDOW WHERE BOTH SEXES EXPERIENCE
753 MULTISENSORY NEUROPLASTICITY

754 One of the most important findings of this study is that most of the neuroplasticity changes start
755 during the photosensitive phase. Despite widespread structural sexual dimorphism, the majority of
756 the structural seasonal neuroplasticity occurs similarly in males and females. A second major
757 observation is that the SCS, various sensory systems and the cerebellum display neuroplasticity in both
758 sexes. This finding fits with a prior histological study that reported volume changes in song control
759 nuclei during the photosensitive phase of male starlings (Riters et al., 2002). During the photosensitive
760 period, aromatase expression is increased and 5β-reductase (which inactivates testosterone) is
761 decreased in the telencephalon (Riters et al., 2001). This indicates that local changes in testosterone
762 metabolism in the brain, could contribute to singing behavior and neuroplasticity changes during the
763 photosensitive period, even though circulating testosterone levels are still low. In line with male
764 starlings, male photosensitive canaries' HVC volume was not significantly different from
765 photostimulated males, which the authors related to a gradual increase in GnRH expression in the
766 POA during the photosensitive period (Hurley et al., 2008).

767 Just like starlings, canaries are open-ended learners. However, canaries modify their song between
768 breeding seasons (when their testosterone levels are low); once they reach a stable song it remains
769 stable for the rest of the breeding season (Nottebohm et al., 1986). Recently, it was shown that this
770 song stabilization is associated with an increase in the perineuronal nets (PNN) expression in RA and
771 Area X of adult male canaries prior to the breeding season (Cornez et al., 2020). They hypothesized
772 that the changes in PNN expression were associated with the closing and re-opening of a sensitive
773 period for vocal learning. We hypothesize that a similar pattern of closing and re-opening of sensitive
774 windows exists in starlings. Among open-ended learners, starlings are more plastic compared to
775 canaries, that is, they can learn new song elements throughout the year and can incorporate them in

36

776   their song up to eighteen months after first hearing them (Böhner et al., 1990; Marler et al., 1994).

777   However, these experiences only result in long-lasting structural changes in the brain during the

778   photosensitive period, which persist during the photostimulated phase and dissipate again in the

779   photorefractory state. As in canaries, male starlings have higher percentage of PNN surrounding PV in

780   the HVC during the photosensitive and photostimulated phase compared to the photorefractory state

781   (Cornez et al., 2017). This indicates that PNNs could play a role in ending a sensitive period. However,

782   compared to other open-ended learners (canaries) and closed-ended learners (zebra finches),

783   starlings exhibit dramatically less PNN expression in their song control system (Cornez et al., 2017).

784   This could be linked to the starling's ability to change its repertoire throughout the year. The relatively

785   low PNN density in the starling brain does not necessarily mean that they cannot use other

786   mechanisms to end their sensitive period. Myelination is another relevant mechanism by which the

787   connectivity of a circuit is consolidated when a sensitive window closes (Knudsen, 2004; Xin and Chan,

788   2020). Using in vivo DTI, which is sensitive to changes in myelination, we demonstrated that both sexes

789   experienced differential and parallel-heightened multisensory neuroplasticity in auditory and visual

790   system and cerebellum mainly during the photosensitive period. This often-neglected period in which

791   gonadal hormones are still very low might represent a 'sensitive window', during which different

792   sensory and motor systems in both telencephalon and cerebellum are seasonally re-shaped. These

793   findings open new vistas for investigating reopening of sensitive or critical periods of neuroplasticity.

5   MATERIAL & METHODS

5.1   SUBJECTS & EXPERIMENTAL SETUP

796   All experiments were performed on thirteen male and twelve female starlings (*Sturnus vulgaris*) that

797   were wild caught as adults in Normandy (France) and Nicosia (Cyprus) in November 2014 and March

798   2017, respectively. All subjects were housed in large indoor aviaries (L x W x H: 2.2 x 1.4 x 2.1 m) at

799   the University of Antwerp with food and water available *ad libitum* and an artificial light-dark cycle

800   mimicking the natural photoperiod. All birds were kept on a long day photoperiod (16h light: 8h dark,

801   16L:8D) in order to induce photorefractory state at the start of experiment. When all birds molted and

802   were fully photorefractory, a first baseline measurement was made. This was in May 2015 for the male

803   starlings, and December 2017 for the female starlings. Both males and females followed the same

804   photoperiodic regime: after the photorefractory baseline scan, they were switched from long to short

805   (8L:16D) days to induce photosensitivity. After twelve weeks of short days, the photosensitive starlings

806   were switched back to long days (16L:8D) to induce photostimulation. They remained on long days,

807   so that they became photorefractory once more. We monitored neuroplasticity repeatedly at six

37

808   different time points. The first time point was at the end of the photorefractory state (PR). After

809   switching to short days, we measured every four weeks to follow up the SEASONAL plasticity during

810   the photosensitive period (SD4, SD8, SD12). Additionally, we measured after four weeks on long days

811   (LD4), when starlings were fully photostimulated. Finally, we measured after sixteen weeks on long

812   days (LD16), when starlings are photorefractory again. At each time point, birds were weighed, songs

813   were recorded, blood samples were taken, and MRI (DTI and 3D scans) was acquired. The housing and

814   experimental procedures were performed in agreement with the European directives, Belgian and

815   Flemish laws and were approved by the Committee on Animal Care and Use of the University of

816   Antwerp, Belgium (2014-52).

5.2   TESTOSTERONE AND ESTROGEN ASSAY

818   Blood samples were collected to quantify plasma testosterone concentration in all birds. In female

819   starlings, we also assayed estradiol in addition to testosterone, since this is one of the primary female

820   sex hormones. At each time point, blood collection occurred within a 2-hour window at noon between

821   11:30h and 13:00h in order to limit variation of plasma levels due to a circadian rhythm. Starlings were

822   housed individually for song recording, which allowed fast capture and blood sampling (within 5 min.

823   of capture) to minimize the increase in testosterone as a result of acute stress (Van Hout et al., 2010).

824   The alar wing vein was punctured with a 25-gauge needle to collect 300–500 µl of blood into heparin-

825   coated capillary tubes. The blood was transferred to tubes and centrifuged for 10 min at 2060g while

826   cooling to 4°C. Plasma was collected and stored at −20 °C prior to assay. Estradiol and testosterone

827   concentrations were quantified by Radioimmunoassay (RIA) using a commercial double antibody

828   system (MP Biomedicals, Solon, Ohio). The estradiol RIA does not cross-react significantly with other

829   estrogens beside estradiol-17β (Estrone: 20% and Estriol 1.51%; all other steroids: <1%) and the intra-

830   assay coefficient of variation is 4.7–10.6%. The testosterone RIA does not significantly cross-react with

831   other androgens beside testosterone (5α-dihydrotestosterone: 3.4%; 5α-androstane-3β, 17β-diol:

832   2.2%; 11-oxo-testosterone: 2%; all other steroids: <1%) and the intra-assay coefficient of variation is

833   4.6–9.1%.

5.3   SONG RECORDING AND ANALYSIS

835   At each MRI imaging time point, songs of all birds were recorded for 2 days, so that we could

836   accurately monitor the evolution of the song behavior in relation to the hormone and neuroplasticity

837   changes. Since isolated starlings do not sing as they would do in groups, we temporarily housed the

838   starlings individually in cages that were placed next to the aviary. Each cage was equipped with a

839   Behringer C-2 condensator microphone placed on top, which was connected to a PR8E multi-channel

840 preamplifier (SM Pro audio), 'Delta Series' Breakout box (M-audio), and a personal computer with

841 Sound Analysis Pro (SAP) software version 2011.104 (http://soundanalysispro.com/) for automated

842 song detection. Due to technical issues, songs of PR and SD12 of male birds were lost.

843 For each bird at each time point, song recordings of four consecutive hours in the morning were

844 analyzed using Raven Pro 1.5 (Cornell Lab of Ornithology, Ithaca, NY). We created sonograms that

845 were acoustically and visually inspected to identify individual songs (N=881) from the background

846 noise of the aviary based on their intensity and the spectral definition. In line with prior song

847 processing studies (Eens, 1997; Van Hout et al., 2012), we defined a song bout as a period of at least

848 5 s of song with pauses no longer than 1.5 s. Starling song consists of a series of distinct song elements

849 or phrases, which can be allocated to 4 categories of phrase types that are mostly performed in a fixed

850 order. The song often starts with one or several whistles (whistle phrase type), followed by a section

851 of complex phrases (variable phrase type) and rapid series of clicks or rattles (rattle phrase type),

852 before ending the song with high frequency song elements (high frequency phrases type). Song bouts

853 containing at least three different phrase types were labeled as 'complete song bouts'.

854 The number of complete song bouts sung per hour within the 4-hour period was taken as a measure

855 of the song rate. We used the first 20 complete song bouts sung within this 4-hour period to calculate

856 the song bout length. This way, we avoided the overrepresentation of songs during time points where

857 the song rate was high.

5.4 MRI DATA ACQUISITION

859 The birds were initially anesthetized using 2% Isoflurane (Isoflo ®, Abbot Laboratories Ltd.) with a

860 mixture of oxygen and nitrogen at flow rates of 100 and 200 cm³/min, respectively. Throughout the

861 imaging procedure, the anesthesia was gradually reduced to 1% Isoflurane in response to their

862 respiration rate, which was monitored with a small pneumatic sensor (SA Instruments, NY, USA)

863 positioned under the bird. Body temperature was monitored with a cloacal temperature probe and

864 kept within a narrow physiological range ((41.0 ± 0.2) °C) using a warm air system with a feedback unit

865 (SA Instruments, NY, USA).

866 All MRI measurements were performed on a 7T horizontal MR system (Pharmascan 70/16 US, Bruker

867 Biospin, Germany). In each imaging session, we acquired a T2-weighted 3D anatomical Rapid

868 acquisition with relaxation enhancement (RARE) scan (3D; TR: 2000 ms; TE_{eff}: 44 ms; RARE factor: 8;

869 acquisition matrix of (256x92x64) giving a voxel resolution of (0.089 x 0.250 x 0.250) mm³).

870 Subsequently, a 4 shot spin-echo echo-planar imaging (SE-EPI) diffusion-weighted (DW) scan (TR: 7000

871 ms; TE: 23 ms; δ 4ms, Δ 12ms; b-value 670 s/mm²; 60 diffusion gradient directions; spatial resolution:

872 (0.179 x 0.179 x 0.350) mm³; 28 coronal slices) was acquired. The 60 diffusion gradient directions were

873 divided over 3 scans, each starting with the acquisition of 7 b0 images. Total acquisition time of all

874 MRI scans amounted to 50 min. After the scanning session, birds were left to recover in a warmed

875 recovery box before returning to the song recording cages next to the aviary.

5.5 MRI DATA PROCESSING

877 Whole-brain volume was manually delineated on the T2-weighted 3D anatomical RARE scan, which

878 covered the entire brain, including telencephalon, diencephalon, mesencephalon and

879 metencephalon. These volumes were used as a measure of brain size, used in further statistical

880 analysis.

881 DW-images were prepared for voxel-based analysis using MRtrix3 version 3.0 (Tournier et al., 2012).

882 We used an in-house algorithm to convert the Bruker 2dseq files to nifti files, which are compatible

883 with other software programs such as SPM and MRtrix3. This step includes a signal scale correction,

884 since the DWI data is acquired in three separate sequential scans. Furthermore, all DW-images were

885 scaled by factor a 10 in 3 dimensions, to enable proper processing of small brains in software programs

886 designed to process human data like SPM and MRtrix3. Voxel-based analysis requires that all images

887 are spatially normalized to the same template, to enable voxel-wise comparisons. A simplified

888 overview of the different MRI data processing steps is given in figure 1B-D.

5.5.1 DTI processing

890 Preprocessing the diffusion data for voxel-based analysis was performed using MRtrix3 (Tournier et

891 al., 2012). First, diffusion gradient orientations were checked and automatically corrected to match

892 the coordinate frame of MRtrix3 and ensure the best global 'connectivity' (Jeurissen et al., 2014a).

893 Since the DTI data is acquired in three separate sequential scans, we further corrected for intensity

894 differences between scans by rescaling the diffusion scans based on their b0 images. Preprocessing of

895 the individual DW-images included the following steps: denoising (Veraart et al., 2016), correction for

896 Gibbs ringing (Kellner et al., 2016), motion and distortion correction using FSL (Andersson and

897 Sotiropoulos, 2016; Jenkinson et al., 2012), bias field correction using ANTS (Advanced Normalization

898 Tool; (Avants et al., 2010)), creating an automated whole-brain mask for whole-brain extraction that

899 were manually checked, upsampling to isotropic voxels of 1.75 mm. These preprocessed diffusion-

900 weighted images were used to calculate individual diffusion maps (FA, MD, AD, and RD). The

901 transformation parameters derived from building the FOD template (see 5.5.2) were applied to the

902 diffusion maps to warp them into the template space to perform voxel-based analysis. Next, these

903 images were smoothed to double voxel size ($3.5 \times 3.5 \times 3.5$ mm³). Finally, all normalized diffusion maps

904 were averaged to create an FA template that is used as a background to display the statistical results.

905 ### 5.5.2   Fixel based analysis

906   For calculation of the fiber-based metrics, we followed the preprocessing steps as defined in (Raffelt

907   et al., 2017). Fixel based analysis follows the same preprocessing steps as DTI processing up until the

908   bias field correction. Apparent fiber density analysis differs from DTI analysis by the fact that it is

909   related to the diffusion-weighted signal intensity within a given voxel. Therefore, global intensity

910   normalization is performed to ensure robust voxel-wise comparison across subjects. Within this step,

911   we used the default FA threshold of 0.4 to create an approximate WM mask, which is used to

912   normalize the median white matter b=0 intensity across all subjects (Raffelt et al., 2012). For each

913   image, a white matter response function was estimated for spherical deconvolution using the

914   unsupervised Dhollander algorithm (Dhollander et al., 2019). Next, the average of all individual

915   response functions was calculated and used for constrained spherical deconvolution to estimate FOD

916   images (Jeurissen et al., 2014b). These FOD images were normalized to create an unbiased study-

917   based FOD template, which involves linear and non-linear registration (Raffelt et al., 2011).

918   Next, the fixels in the FOD template are thresholded at 0.15, identifying the template white matter

919   fixels to be included in further analysis. This threshold is lower than the default threshold of 0.25 for

920   the human brain, as this threshold is too high for the songbird brain and excludes many of the genuine

921   white matter fibers. We are aware that choosing a lower threshold comes with the risk of introducing

922   noisy fixels, especially within grey matter, and consider this in the interpretation of the results.

923   The estimated transformation parameters or warps of each subject to the template were used to

924   transform the individual FOD maps into template space without FOD reorientation, so that the

925   apparent FD can be estimated prior to reorienting the fixels. In the next step, we compare the fixels

926   within a spatially matching voxel of the individual subject and the template white matter fixels, to

927   identify which fixels correspond to each other and subsequently assign the corresponding FD value

928   (Raffelt et al., 2017).

929   Next to FD, we also computed a fixel-based metric related to the macroscopic morphology in fiber

930   bundle cross-section (FC). Fiber bundle cross-section (FC) information relies solely on the

931   transformation parameters or Jacobian determinants generated during the construction of the

932   population template, similar to other morphometry analyses like voxel-based morphometry

933   (Ashburner and Friston, 2000). Morphological differences in the plane perpendicular to the fixel

934   orientation could reflect differences in the number of axons, myelination, or the spacing between

935   axons. For group statistical analysis, the FC values were logarithmically transformed to log FC to ensure

936   that the data are centered on zero and normally distributed. Positive values indicate then expansion,

937 whereas negative values reflect shrinkage of a fiber bundle relative to the template (Raffelt et al.,
938 2017).

5.5.3   Tractography

940 A whole-brain tractogram was generated from the FOD template, which is required for statistical
941 analysis using connectivity-based fixel enhancement (CFE) (Raffelt et al., 2015). We created 20 million
942 tracks using dynamic seeding, and maximum angle of 45°. We used Spherical-deconvolution informed
943 filtering (SIFT) to filter our tractogram to ensure that the streamline densities approximate the
944 biological fiber densities estimated by spherical deconvolution. SIFT2 creates for each streamline a
945 weighting coefficient based on the underlying FOD (Smith et al., 2015). Currently, track-weights
946 created in SIFT2 cannot be implicated in statistical analysis. Therefore, in our statistical analyses we
947 used SIFT, which selectively filters out streamlines based on the spherical deconvolution to reduce the
948 tractogram to 2 million tracks (Smith et al., 2013).

5.6   STATISTICAL ANALYSIS

950 Voxel-based statistical analyses allow for unbiased determination of sexual dimorphisms, longitudinal
951 changes over time and the neural correlates of song behavior (performed using SPM12). To examine
952 group level repeated measurements in a voxel-based manner using the standard general linear model
953 approach as implemented in SPM and FSL, we followed the recommendations of McFarquhar (2019).
954 Effects of sex and brain size are assessed using full factorial design, whereas the effect of time and the
955 interaction between sex and time are assessed using a flexible factorial design in SPM.

956 Voxel-based clusters are further explored by extracting the average values from these statistical ROI
957 clusters and investigate either their change over time or their correlation to a certain song parameter.
958 Traditional correlation techniques like Pearson correlation require independence of data. Since we
959 have repeated measures, this assumption of independence is violated when performing a multiple
960 regression on longitudinal data. Traditionally this is solved by using data from only one time point.
961 However, a lot of information on temporal changes is lost this way. Therefore, we use repeated
962 measures correlation instead of traditional correlation techniques (Bakdash and Marusich, 2017). This
963 way, we can assess the within-subject correlation, which gives a meaningful interpretation of how
964 testosterone, song and diffusion parameters correlate to each other on a within-subject level.

965 Hormone levels, brain size and song parameters were analyzed using linear mixed model in JMP Pro
966 13 (SAS Institute Inc., Cary, NC, 1989-2007) to assess the main effect of time, sex and their interaction.

5.6.1   Song analysis and plasma testosterone and estrogen concentrations

967 We investigated whether brain size, song behavior, testosterone and estrogen levels changed
968 significantly over time using linear mixed model ('time point', 'sex' and the interaction 'sex * time
969 point' as fixed factors and 'subject ID' as a random factor) via JMP Pro 13 (SAS Institute Inc., Cary, NC,
970 1989-2007). Tukey's Honest Significant Difference (HSD) was used for *post hoc* statistical testing to
971 correct for multiple comparison.

973 Subsequently, within-subject correlations between testosterone and song parameters were assessed
974 by using the repeated measures correlation package (rmcorr in R) (Bakdash and Marusich, 2017).
975 Differences were considered significant for $p < 0.05$.

5.6.2   Statistical analysis brain size

977 To investigate the role of brain size on the general sexual dimorphism and on song behavior, we
978 artificially divided the starlings by their brain size using a median split analogous to the analysis in
979 Kurth et al. (2018). Birds with a brain size larger than the median brain size of 1805 mm³ were
980 considered as large brain starlings. This way, we divided females in large and small brain groups
981 (respectively, females: N=6 large and N=6 small, males N=6 large, N=7 small). In order to test whether
982 song or testosterone change differently in large versus small brain birds, we performed a linear mixed
983 model analysis for each sex separately with time, brain size (categorical factor of 2 levels) and their
984 interaction as fixed factors and subject as a random factor. Post hoc testing in the linear mixed model
985 analysis was corrected with HSD for multiple comparison using JMP Pro 13. Brain size (continuous
986 variable), body weight and song parameters were averaged over time to perform a Pearson
987 correlation between these factors for each sex separately in JMP Pro 13.

5.6.3   Voxel-based analyses

989 To identify the general sexual dimorphisms between male and female starlings, we first performed a
990 full factorial voxel-based analysis within the entire brain using SPM12. The same full factorial design
991 was used in the voxel-based analysis for categorical brain size difference with the caveat that brain
992 size was substituted as a factor instead of sex. In a separate analysis, we determined the longitudinal
993 neuroplasticity changes over time within the song control system, auditory system and their
994 interconnecting tracts using a flexible factorial analysis. To investigate where within the starling brain
995 microstructural properties relate to song behavior parameters, we executed voxel-based multiple
996 regression analyses for FA. To this end, the averaged song behavior parameters were used for this
997 analysis. Clusters were only considered significant if their peak value reached the significance level of
998 $p < 0.05$ corrected for the familywise error rate (FWE) and contained at least (k_E) 10 (contiguous) voxels.
999 Flexible factorial and multiple regression analyses were performed with a small volume mask including

43

1000 the song control nuclei, auditory system and their interconnecting tracts. This way, we ensured we did

1001 not miss significant changes in relevant regions that might be obscured by the stringent correction for

1002 multiple comparisons in whole-brain analysis. Results shown are from the voxel-based analysis with

1003 the latter small volume correction. Results were displayed with a significance threshold of $p<0.001$

1004 (uncorrected for multiple comparison) and overlaid to a group-average FA map (average of all spatially

1005 normalized FA maps, including all subjects and time points).

1006 Significant clusters were converted to ROIs (cluster-based ROIs) of which the average diffusion

1007 parameters (FA, MD, AD and RD) and fixel based parameters (FD and log FC) were extracted. In order

1008 to determine the extent of the overall association between diffusion parameters and song rate,

1009 Pearson's correlation was calculated using JMP Pro 13 (SAS Institute Inc., Cary, NC, 1989-2007).

1010 Further in depth analysis was performed to determine if this overall association was also caused by a

1011 within-subject correlation by using rmcorr in R (Bakdash and Marusich, 2017).

1012 ### 5.6.4   Fixel-based analysis

1013 Fixel-based statistical analysis was performed using the connectivity-based fixel enhancement (CFE)

1014 described by (Raffelt et al., 2015). A connectivity matrix was calculated using the fixel template and

1015 SIFT filtered tractogram. This connectivity matrix was used to perform connectivity-based smoothing

1016 where only fixels belonging to the same fiber tract are smoothed, instead of the neighboring voxels as

1017 in a voxel-based analysis. A fixel-based analysis was performed to assess the difference between sexes

1018 and brain size, both examined in separate tests. In the CFE statistical test, we used whole block

1019 exchangeability to look for changes between subjects and included the time point information in a

1020 variance group. Similarly to the voxel-based DTI analysis, statistical results were visualized with a

1021 significance threshold of $p<0.001$ (uncorrected for multiple comparison) and color-coded according to

1022 their significance T-value or the physical direction of the tract.

6   ACKNOWLEDGMENTS

7 REFERENCES:

Adret-Hausberger, M., 1994. Seasonal variation in the whistles of the starling sturnus vulgaris. Ibis 126, 372-378.

Alward, B.A., Balthazart, J., Ball, G.F., 2013. Differential effects of global versus local testosterone on singing behavior and its underlying neural substrate. Proc Natl Acad Sci U S A 110, 19573-19578.

Andersson, J.L.R., Sotiropoulos, S.N., 2016. An integrated approach to correction for off-resonance effects and subject movement in diffusion MR imaging. Neuroimage 125, 1063-1078.

Arends, J.J.A., Zeigler, H.P., 1991. Organization of the cerebellum in the pigeon (Columba livia): I. Corticonuclear and corticovestibular connections. Journal of Comparative Neurology 306, 221-244.

Ashburner, J., Friston, K.J., 2000. Voxel-based morphometry--the methods. Neuroimage 11, 805-821.

Avants, B.B., Yushkevich, P., Pluta, J., Minkoff, D., Korczykowski, M., Detre, J., Gee, J.C., 2010. The optimal template effect in hippocampus studies of diseased populations. Neuroimage 49, 2457-2466.

Bailey, D.J., Saldanha, C.J., 2015. The importance of neural aromatization in the acquisition, recall, and integration of song and spatial memories in passerines. Hormones and behavior 74, 116-124.

Bailey, D.J., Wade, J., 2003. Differential expression of the immediate early genes FOS and ZENK following auditory stimulation in the juvenile male and female zebra finch. Molecular Brain Research 116, 147-154.

Bailey, D.J., Wade, J., Saldanha, C.J., 2009. Hippocampal lesions impair spatial memory performance, but not song--a developmental study of independent memory systems in the zebra finch. Dev Neurobiol 69, 491-504.

Bakdash, J.Z., Marusich, L.R., 2017. Repeated Measures Correlation. Front Psychol 8, 456.

Beaulieu, C., 2002. The basis of anisotropic water diffusion in the nervous system - a technical review. NMR Biomed 15, 435-455.

Beaulieu, C., 2014. The Biological Basis of Diffusion Anisotropy. 155-183.

Bennett, A.T., Cuthill, I.C., Partridge, J.C., Lunau, K., 1997. Ultraviolet plumage colors predict mate preferences in starlings. Proc Natl Acad Sci U S A 94, 8618-8621.

Bentley, G.E., Tucker, S., Chou, H., Hau, M., Perfito, N., 2013. Testicular growth and regression are not correlated with Dio2 expression in a wild male songbird, sturnus vulgaris, exposed to natural changes in photoperiod. Endocrinology 154, 1813-1819.

Bernard, D.J., Ball, G.F., 1997. Photoperiodic condition modulates the effects of testosterone on SCS nuclei volumes in male starlings. General and comparative endocrinology 105, 276-283.

Bernard, D.J., Casto, J.M., Ball, G.F., 1993. Sexual dimorphism in the volume of song control nuclei in European starlings: Assessment by a Nissl stain and autoradiography for muscarinic cholinergic receptors. The Journal of comparative neurology 334, 559-570.

Bernard, D.J., Eens, M., Ball, G.F., 1996. Age- and behavior-related variation in volumes of song control nuclei in male European starlings. J Neurobiol 30, 329-339.

Böhner, J., Chaiken, M.L., Ball, G.F., Marler, P., 1990. Song acquisition in photosensitive and photorefractory male European starlings. Hormones and behavior 24, 582-594.

Bosíková, E., Kostal, L., Kubikova, L., 2010. Birdsong: From behaviour to brain. Biologia 65, 379-387.

Clarke, P.G.H., 1977. Some visual and other connections to the cerebellum of the pigeon. Journal of Comparative Neurology 174, 535-552.

Cornez, G., Collignon, C., Müller, W., Ball, G.F., Cornil, C.A., Balthazart, J., 2020. Seasonal changes of perineuronal nets and song learning in adult canaries (Serinus canaria). Behavioural Brain Research 380, 112437.

Cornez, G., Madison, F.N., Van der Linden, A., Cornil, C., Yoder, K.M., Ball, G.F., Balthazart, J., 2017. Perineuronal nets and vocal plasticity in songbirds: A proposed mechanism to explain the difference between closed-ended and open-ended learning. Dev Neurobiol 77, 975-994.

D'Angelo, E., 2018. Physiology of the cerebellum. Handb Clin Neurol 154, 85-108.

1079   Dawson, A., 1983. Plasma gonadal steroid levels in wild starlings (Sturnus vulgaris) during the annual
1080   cycle and in relation to the stages of breeding. General and comparative endocrinology 49, 286-294.
1081   De Groof, G., Balthazart, J., Cornil, C.A., Van der Linden, A., 2017. Topography and Lateralized Effect
1082   of Acute Aromatase Inhibition on Auditory Processing in a Seasonal Songbird. J Neurosci 37, 4243-
1083   4254.
1084   De Groof, G., Gwinner, H., Steiger, S., Kempenaers, B., Van der Linden, A., 2010. Neural correlates of
1085   behavioural olfactory sensitivity changes seasonally in European starlings. PLoS One 5, e14337.
1086   De Groof, G., Poirier, C., George, I., Hausberger, M., Van der Linden, A., 2013. Functional changes
1087   between seasons in the male songbird auditory forebrain. Front Behav Neurosci 7, 196.
1088   De Groof, G., Verhoye, M., Van Meir, V., Balthazart, J., Van der Linden, A., 2008. Seasonal rewiring of
1089   the songbird brain: an in vivo MRI study. Eur J Neurosci 28, 2475-2485; discussion 2474.
1090   De Groof, G., Verhoye, M., Van Meir, V., Tindemans, I., Leemans, A., Van der Linden, A., 2006. In vivo
1091   diffusion tensor imaging (DTI) of brain subdivisions and vocal pathways in songbirds. Neuroimage 29,
1092   754-763.
1093   Dean, S.L., McCarthy, M.M., 2008. Steroids, sex and the cerebellar cortex: implications for human
1094   disease. Cerebellum (London, England) 7, 38-47.
1095   Dhollander, T., Mito, R., Raffelt, D., Connelly, A., 2019. Improved white matter response function
1096   estimation for 3-tissue constrained spherical deconvolution. Proc Intl Soc Mag Reson Med 27.
1097   Eens, M., 1997. Understanding the Complex Song of the European Starling: An Integrated Ethological
1098   Approach. 26, 355-434.
1099   Genc, S., Tax, C.M.W., Raven, E.P., Chamberland, M., Parker, G.D., Jones, D.K., 2020. Impact of b-
1100   value on estimates of apparent fibre density. Hum Brain Mapp 41, 2583-2595.
1101   Gobes, S.M.H., ter Haar, S.M., Vignal, C., Vergne, A.L., Mathevon, N., Bolhuis, J.J., 2009. Differential
1102   responsiveness in brain and behavior to sexually dimorphic long calls in male and female zebra
1103   finches. Journal of Comparative Neurology 516, 312-320.
1104   Hall, Z.J., Macdougall-Shackleton, S.A., 2012. Influence of testosterone metabolites on song-control
1105   system neuroplasticity during photostimulation in adult European starlings (Sturnus vulgaris). PLoS
1106   One 7, e40060.
1107   Hamaide, J., De Groof, G., Van Ruijssevelt, L., Lukacova, K., Van Audekerke, J., Verhoye, M., Van der
1108   Linden, A., 2018a. Volumetric development of the zebra finch brain throughout the first 200 days of
1109   post-hatch life traced by in vivo MRI. Neuroimage 183, 227-238.
1110   Hamaide, J., De Groof, G., Van Steenkiste, G., Jeurissen, B., Van Audekerke, J., Naeyaert, M., Van
1111   Ruijssevelt, L., Cornil, C., Sijbers, J., Verhoye, M., Van der Linden, A., 2017. Exploring sex differences
1112   in the adult zebra finch brain: In vivo diffusion tensor imaging and ex vivo super-resolution track
1113   density imaging. Neuroimage 146, 789-803.
1114   Hamaide, J., Lukacova, K., Orije, J., Keliris, G.A., Verhoye, M., Van der Linden, A., 2020. In vivo
1115   assessment of the neural substrate linked with vocal imitation accuracy. Elife 9.
1116   Hamaide, J., Lukacova, K., Van Audekerke, J., Verhoye, M., Kubikova, L., Van der Linden, A., 2018b.
1117   Neuroplasticity in the cerebello-thalamo-basal ganglia pathway: A longitudinal in vivo MRI study in
1118   male songbirds. Neuroimage 181, 190-202.
1119   Hanggi, J., Fovenyi, L., Liem, F., Meyer, M., Jancke, L., 2014. The hypothesis of neuronal
1120   interconnectivity as a function of brain size-a general organization principle of the human
1121   connectome. Front Hum Neurosci 8, 915.
1122   Healy, S.D., Rowe, C., 2007. A critique of comparative studies of brain size. Proc Biol Sci 274, 453-
1123   464.
1124   Hurley, L.L., Wallace, A.M., Sartor, J.J., Ball, G.F., 2008. Photoperiodic induced changes in
1125   reproductive state of border canaries (Serinus canaria) are associated with marked variation in
1126   hypothalamic gonadotropin-releasing hormone immunoreactivity and the volume of song control
1127   regions. General and comparative endocrinology 158, 10-19.
1128   Ito, M., 2006. Cerebellar circuitry as a neuronal machine. Progress in Neurobiology 78, 272-303.

1129 Iwaniuk, A.N., Hurd, P.L., Wylie, D.R., 2007. Comparative morphology of the avian cerebellum: II. Size
1130 of folia. Brain Behav Evol 69, 196-219.
1131 Jarvis, E.D., Gunturkun, O., Bruce, L., Csillag, A., Karten, H., Kuenzel, W.J., Medina, L., Paxinos, G.,
1132 Perkel, D.J., Shimizu, T., Striedter, G., Wild, J.M., Ball, G.F., Dugas-Ford, J., Durand, S.E., Hough, G.E.,
1133 Husband, S., Kubikova, L., Lee, D.W., Mello, C.V., Powers, A., Siang, C., Smulders, T., Wada, K., White,
1134 S.A., Yamamoto, K., Yu, J., Reiner, A., Butler, A.B., 2005. Avian brains and a new understanding of
1135 vertebrate brain evolution. Nat Rev Neurosci 6, 151-159.
1136 Jenkinson, M., Beckmann, C.F., Behrens, T.E., Woolrich, M.W., Smith, S.M., 2012. Fsl. Neuroimage
1137 62, 782-790.
1138 Jeurissen, B., Leemans, A., Sijbers, J., 2014a. Automated correction of improperly rotated diffusion
1139 gradient orientations in diffusion weighted MRI. Med Image Anal 18, 953-962.
1140 Jeurissen, B., Tournier, J.D., Dhollander, T., Connelly, A., Sijbers, J., 2014b. Multi-tissue constrained
1141 spherical deconvolution for improved analysis of multi-shell diffusion MRI data. Neuroimage 103,
1142 411-426.
1143 Karten, H.J., Brzozowska-Prechtl, A., Lovell, P.V., Tang, D.D., Mello, C.V., Wang, H., Mitra, P.P., 2013.
1144 Digital atlas of the zebra finch (Taeniopygia guttata) brain: a high-resolution photo atlas. The Journal
1145 of comparative neurology 521, 3702-3715.
1146 Kellner, E., Dhital, B., Kiselev, V.G., Reisert, M., 2016. Gibbs-ringing artifact removal based on local
1147 subvoxel-shifts. Magn Reson Med 76, 1574-1581.
1148 Knudsen, E.I., 2004. Sensitive Periods in the Development of the Brain and Behavior. Journal of
1149 Cognitive Neuroscience 16, 1412-1425.
1150 Konopka, G., Roberts, T.F., 2016. Insights into the Neural and Genetic Basis of Vocal Communication.
1151 Cell 164, 1269-1276.
1152 Kosarussavadi, S., Pennington, Z.T., Covell, J., Blaisdell, A.P., Schlinger, B.A., 2017. Across sex and
1153 age: Learning and memory and patterns of avian hippocampal gene expression. Behavioral
1154 neuroscience 131, 483-491.
1155 Kurth, F., Thompson, P.M., Luders, E., 2018. Investigating the differential contributions of sex and
1156 brain size to gray matter asymmetry. Cortex 99, 235-242.
1157 Larson, T.A., Thatra, N.M., Hou, D., Hu, R.A., Brenowitz, E.A., 2019. Seasonal changes in neuronal
1158 turnover in a forebrain nucleus in adult songbirds. The Journal of comparative neurology 527, 767-
1159 779.
1160 Macphail, E., 2002. The role of the avian hippocampus in spatial memory. Psicológica: Revista de
1161 metodología y psicología experimental, ISSN 0211-2159, Vol. 23, Nº 1, 2002 (Ejemplar dedicado a:
1162 Spatial Learning and Cognition), pags. 93-108 23.
1163 Marien, P., Ackermann, H., Adamaszek, M., Barwood, C.H., Beaton, A., Desmond, J., De Witte, E.,
1164 Fawcett, A.J., Hertrich, I., Kuper, M., Leggio, M., Marvel, C., Molinari, M., Murdoch, B.E., Nicolson,
1165 R.I., Schmahmann, J.D., Stoodley, C.J., Thurling, M., Timmann, D., Wouters, E., Ziegler, W., 2014.
1166 Consensus paper: Language and the cerebellum: an ongoing enigma. Cerebellum 13, 386-410.
1167 Marler, P., BÖHNER, J., Chaiken, M., 1994. Repertoire Turnover and the Timing of Song Acquisition in
1168 European Starlings. Behaviour 128, 25-39.
1169 McFarquhar, M., 2019. Modeling Group-Level Repeated Measurements of Neuroimaging Data Using
1170 the Univariate General Linear Model. Frontiers in neuroscience 13, 352.
1171 Medina, J.F., Repa, J.C., Mauk, M.D., LeDoux, J.E., 2002. Parallels between cerebellum- and
1172 amygdala-dependent conditioning. Nat Rev Neurosci 3, 122-131.
1173 Miall, R.C., Reckess, G.Z., 2002. The Cerebellum and the Timing of Coordinated Eye and Hand
1174 Tracking. Brain and Cognition 48, 212-226.
1175 Nixdorf-Bergweiler, B.E., 1996. Divergent and parallel development in volume sizes of telencephalic
1176 song nuclei in male and female zebra finches. The Journal of comparative neurology 375, 445-456.
1177 Nottebohm, F., Arnold, A.P., 1976. Sexual dimorphism in vocal control areas of the songbird brain.
1178 Science 194, 211-213.

1179 Nottebohm, F., Kelley, D.B., Paton, J.A., 1982. Connections of vocal control nuclei in the canary
1180 telencephalon. The Journal of comparative neurology 207, 344-357.
1181 Nottebohm, F., Nottebohm, M.E., Crane, L., 1986. Developmental and seasonal changes in canary
1182 song and their relation to changes in the anatomy of song-control nuclei. Behavioral and Neural
1183 Biology 46, 445-471.
1184 Ocklenburg, S., Strockens, F., Gunturkun, O., 2013. Lateralisation of conspecific vocalisation in non-
1185 human vertebrates. Laterality 18, 1-31.
1186 Odom, K.J., Hall, M.L., Riebel, K., Omland, K.E., Langmore, N.E., 2014. Female song is widespread and
1187 ancestral in songbirds. Nat Commun 5, 3379.
1188 Orije, J., Cardon, E., de Groof, G., Hamaide, J., Jonckers, E., Van Massenhoven, S., Darras, V.,
1189 Balthazart, J., Verhoye, M., Van der Linden, A., 2020. In vivo online monitoring of testosterone-
1190 induced neuroplasticity in a female songbird. Hormones and behavior 118.
1191 Pavlova, D., Pinxten, R., Eens, M., 2007. Seasonal singing patterns and individual consistency in song
1192 activity in female European starlings (Sturnus vulgaris). Behaviour 144, 663-680.
1193 Person, A.L., Gale, S.D., Farries, M.A., Perkel, D.J., 2008. Organization of the songbird basal ganglia,
1194 including area X. The Journal of comparative neurology 508, 840-866.
1195 Pidoux, L., Le Blanc, P., Levenes, C., Leblois, A., 2018. A subcortical circuit linking the cerebellum to
1196 the basal ganglia engaged in vocal learning. Elife 7.
1197 Raffelt, D., Tournier, J.D., Fripp, J., Crozier, S., Connelly, A., Salvado, O., 2011. Symmetric
1198 diffeomorphic registration of fibre orientation distributions. Neuroimage 56, 1171-1180.
1199 Raffelt, D., Tournier, J.D., Rose, S., Ridgway, G.R., Henderson, R., Crozier, S., Salvado, O., Connelly, A.,
1200 2012. Apparent Fibre Density: a novel measure for the analysis of diffusion-weighted magnetic
1201 resonance images. Neuroimage 59, 3976-3994.
1202 Raffelt, D.A., Smith, R.E., Ridgway, G.R., Tournier, J.D., Vaughan, D.N., Rose, S., Henderson, R.,
1203 Connelly, A., 2015. Connectivity-based fixel enhancement: Whole-brain statistical analysis of
1204 diffusion MRI measures in the presence of crossing fibres. Neuroimage 117, 40-55.
1205 Raffelt, D.A., Tournier, J.D., Smith, R.E., Vaughan, D.N., Jackson, G., Ridgway, G.R., Connelly, A., 2017.
1206 Investigating white matter fibre density and morphology using fixel-based analysis. Neuroimage 144,
1207 58-73.
1208 Reiner, A., Perkel, D.J., Bruce, L.L., Butler, A.B., Csillag, A., Kuenzel, W., Medina, L., Paxinos, G.,
1209 Shimizu, T., Striedter, G., Wild, M., Ball, G.F., Durand, S., Gunturkun, O., Lee, D.W., Mello, C.V.,
1210 Powers, A., White, S.A., Hough, G., Kubikova, L., Smulders, T.V., Wada, K., Dugas-Ford, J., Husband,
1211 S., Yamamoto, K., Yu, J., Siang, C., Jarvis, E.D., Avian Brain Nomenclature, F., 2004. Revised
1212 nomenclature for avian telencephalon and some related brainstem nuclei. The Journal of
1213 comparative neurology 473, 377-414.
1214 Rensel, M.A., Ellis, J.M.S., Harvey, B., Schlinger, B.A., 2015. Sex, estradiol, and spatial memory in a
1215 food-caching corvid. Hormones and behavior 75, 45-54.
1216 Riebel, K., 2016. Understanding Sex Differences in Form and Function of Bird Song: The Importance
1217 of Studying Song Learning Processes. Frontiers in Ecology and Evolution 4.
1218 Riters, L.V., Baillien, M., Eens, M., Pinxten, R., Foidart, A., Ball, G.F., Balthazart, J., 2001. Seasonal
1219 Variation in Androgen-Metabolizing Enzymes in the Diencephalon and Telencephalon of the Male
1220 European Starling (Sturnus vulgaris). Journal of neuroendocrinology 13, 985-997.
1221 Riters, L.V., Eens, M., Pinxten, R., Ball, G.F., 2002. Seasonal changes in the densities of alpha(2)
1222 noradrenergic receptors are inversely related to changes in testosterone and the volumes of song
1223 control nuclei in male European starlings. The Journal of comparative neurology 444, 63-74.
1224 Rogers, L.J., 2012. The two hemispheres of the avian brain: their differing roles in perceptual
1225 processing and the expression of behavior. Journal of Ornithology 153, 61-74.
1226 Rouse, M.L., Jr., Stevenson, T.J., Fortune, E.S., Ball, G.F., 2015. Reproductive state modulates
1227 testosterone-induced singing in adult female European starlings (Sturnus vulgaris). Hormones and
1228 behavior 72, 78-87.

1229 Sagi, Y., Tavor, I., Hofstetter, S., Tzur-Moryosef, S., Blumenfeld-Katzir, T., Assaf, Y., 2012. Learning in
1230 the fast lane: new insights into neuroplasticity. Neuron 73, 1195-1203.
1231 Smith, R.E., Tournier, J.D., Calamante, F., Connelly, A., 2013. SIFT: Spherical-deconvolution informed
1232 filtering of tractograms. Neuroimage 67, 298-312.
1233 Smith, R.E., Tournier, J.D., Calamante, F., Connelly, A., 2015. SIFT2: Enabling dense quantitative
1234 assessment of brain white matter connectivity using streamlines tractography. Neuroimage 119,
1235 338-351.
1236 Smith, S.S., 1995. Sensorimotor-correlated discharge recorded from ensembles of cerebellar Purkinje
1237 cells varies across the estrous cycle of the rat. Journal of Neurophysiology 74, 1095-1108.
1238 Song, S.-K., Sun, S.-W., Ramsbottom, M.J., Chang, C., Russell, J., Cross, A.H., 2002. Dysmyelination
1239 Revealed through MRI as Increased Radial (but Unchanged Axial) Diffusion of Water. NeuroImage 17,
1240 1429-1436.
1241 Song, S.K., Yoshino, J., Le, T.Q., Lin, S.J., Sun, S.W., Cross, A.H., Armstrong, R.C., 2005. Demyelination
1242 increases radial diffusivity in corpus callosum of mouse brain. Neuroimage 26, 132-140.
1243 Stevenson, T.J., Ball, G.F., 2010. Photoperiodic differences in a forebrain nucleus involved in vocal
1244 plasticity: enkephalin immunoreactivity reveals volumetric variation in song nucleus lMAN but not
1245 NIf in male European starlings (Sturnus vulgaris). Dev Neurobiol 70, 751-763.
1246 Stevenson, T.J., Hahn, T.P., Ball, G.F., 2012. Variation in gonadotrophin-releasing hormone-1 gene
1247 expression in the preoptic area predicts transitions in seasonal reproductive state. Journal of
1248 neuroendocrinology 24, 267-274.
1249 Strick, P.L., Dum, R.P., Fiez, J.A., 2009. Cerebellum and nonmotor function. Annu Rev Neurosci 32,
1250 413-434.
1251 Suarez, R., Paolino, A., Fenlon, L.R., Morcom, L.R., Kozulin, P., Kurniawan, N.D., Richards, L.J., 2018. A
1252 pan-mammalian map of interhemispheric brain connections predates the evolution of the corpus
1253 callosum. PNAS 115, 9622-9627.
1254 Tanabe, Y., Nakamura, T., Fujioka, K., Doi, O., 1979. Production and secretion of sex steroid
1255 hormones by the testes, the ovary, and the adrenal glands of embryonic and young chickens (Gallus
1256 domesticus). General and comparative endocrinology 39, 26-33.
1257 Tournier, J.D., Calamante, F., Connelly, A., 2012. MRtrix: Diffusion tractography in crossing fiber
1258 regions. International Journal of Imaging Systems and Technology 22, 53-66.
1259 Tropp, J., Markus, E.J., 2001. Sex differences in the dynamics of cue utilization and exploratory
1260 behavior. Behavioural Brain Research 119, 143-154.
1261 Van Hout, A.J., Eens, M., Balthazart, J., Pinxten, R., 2009. Complex modulation of singing behavior by
1262 testosterone in an open-ended learner, the European Starling. Hormones and behavior 56, 564-573.
1263 Van Hout, A.J., Eens, M., Darras, V.M., Pinxten, R., 2010. Acute stress induces a rapid increase of
1264 testosterone in a songbird: implications for plasma testosterone sampling. General and comparative
1265 endocrinology 168, 505-510.
1266 Van Hout, A.J., Pinxten, R., Darras, V.M., Eens, M., 2012. Testosterone increases repertoire size in an
1267 open-ended learner: an experimental study using adult male European starlings (Sturnus vulgaris).
1268 Hormones and behavior 62, 563-568.
1269 Vates, G.E., Broome, B.M., Mello, C.V., Nottebohm, F., 1996. Auditory pathways of caudal
1270 telencephalon and their relation to the song system of adult male zebra finches. The Journal of
1271 comparative neurology 366, 613-642.
1272 Veraart, J., Novikov, D.S., Christiaens, D., Ades-Aron, B., Sijbers, J., Fieremans, E., 2016. Denoising of
1273 diffusion MRI using random matrix theory. Neuroimage 142, 394-406.
1274 Whitlock, D.G., 1952. A neurohistological and neurophysiological study of afferent fiber tracts and
1275 receptive areas of the avian cerebellum. Journal of Comparative Neurology 97, 567-635.
1276 Wild, J.M., Farabaugh, S.M., 1996. Organization of afferent and efferent projections of the nucleus
1277 basalis prosencephali in a passerine, Taeniopygia guttata. Journal of Comparative Neurology 365,
1278 306-328.

1279   Williams, T.D., Kitaysky, A.S., Vezina, F., 2004. Individual variation in plasma estradiol-17beta and
1280   androgen levels during egg formation in the European starling Sturnus vulgaris: implications for
1281   regulation of yolk steroids. General and comparative endocrinology 136, 346-352.
1282   Wylie, D.R., Gutierrez-Ibanez, C., Gaede, A.H., Altshuler, D.L., Iwaniuk, A.N., 2018. Visual-Cerebellar
1283   Pathways and Their Roles in the Control of Avian Flight. Frontiers in neuroscience 12, 223.
1284   Xin, W., Chan, J.R., 2020. Myelin plasticity: sculpting circuits in learning and memory. Nature Reviews
1285   Neuroscience 21, 682-694.
1286   Yang, L.M., Vicario, D.S., 2015. Exposure to a novel stimulus environment alters patterns of
1287   lateralization in avian auditory cortex. Neuroscience 285, 107-118.
1288   Zatorre, R.J., Fields, R.D., Johansen-Berg, H., 2012. Plasticity in gray and white: neuroimaging
1289   changes in brain structure during learning. Nat Neurosci 15, 528-536.
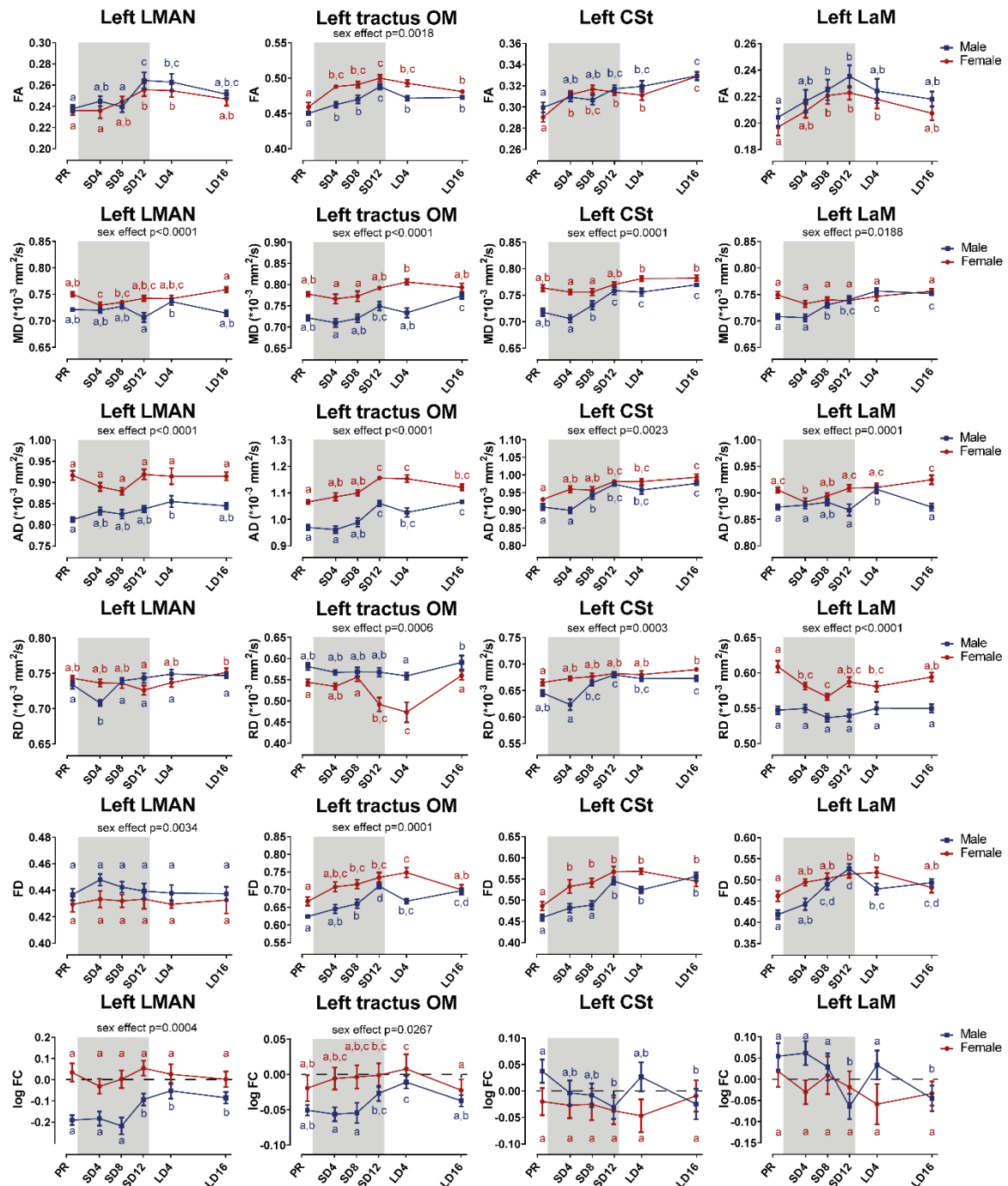
1290

1291

8 SUPPLEMENTARY FIGURES
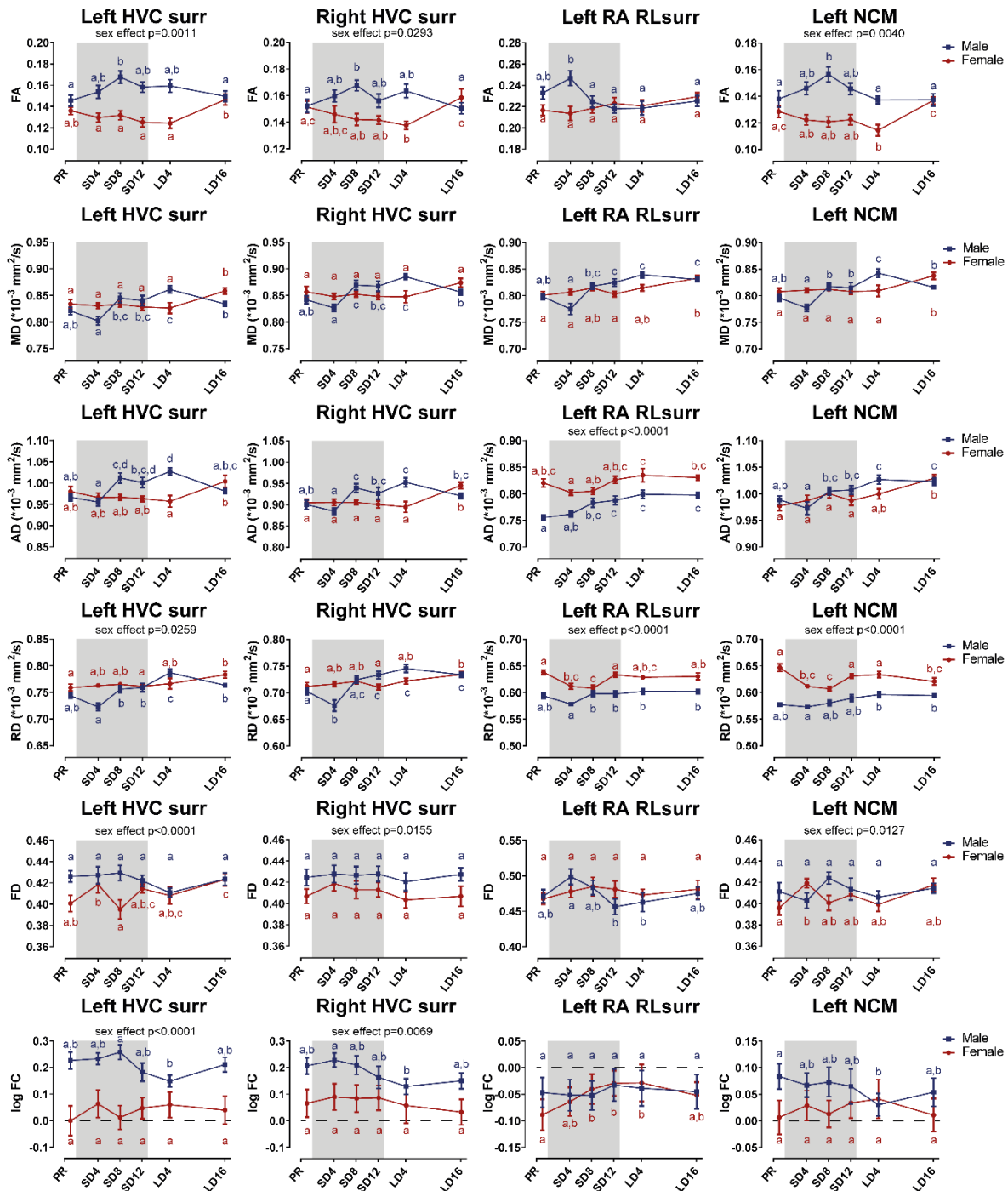
Figure 8 – Figure supplement 1: Summary of the longitudinal changes over time in FA, MD, AD, RD, FD and log FC extracted from ROI-based clusters that had a significant interaction, including HVC surroundings (surr), left RA rostro-lateral surroundings (RLsurr) and NCM.
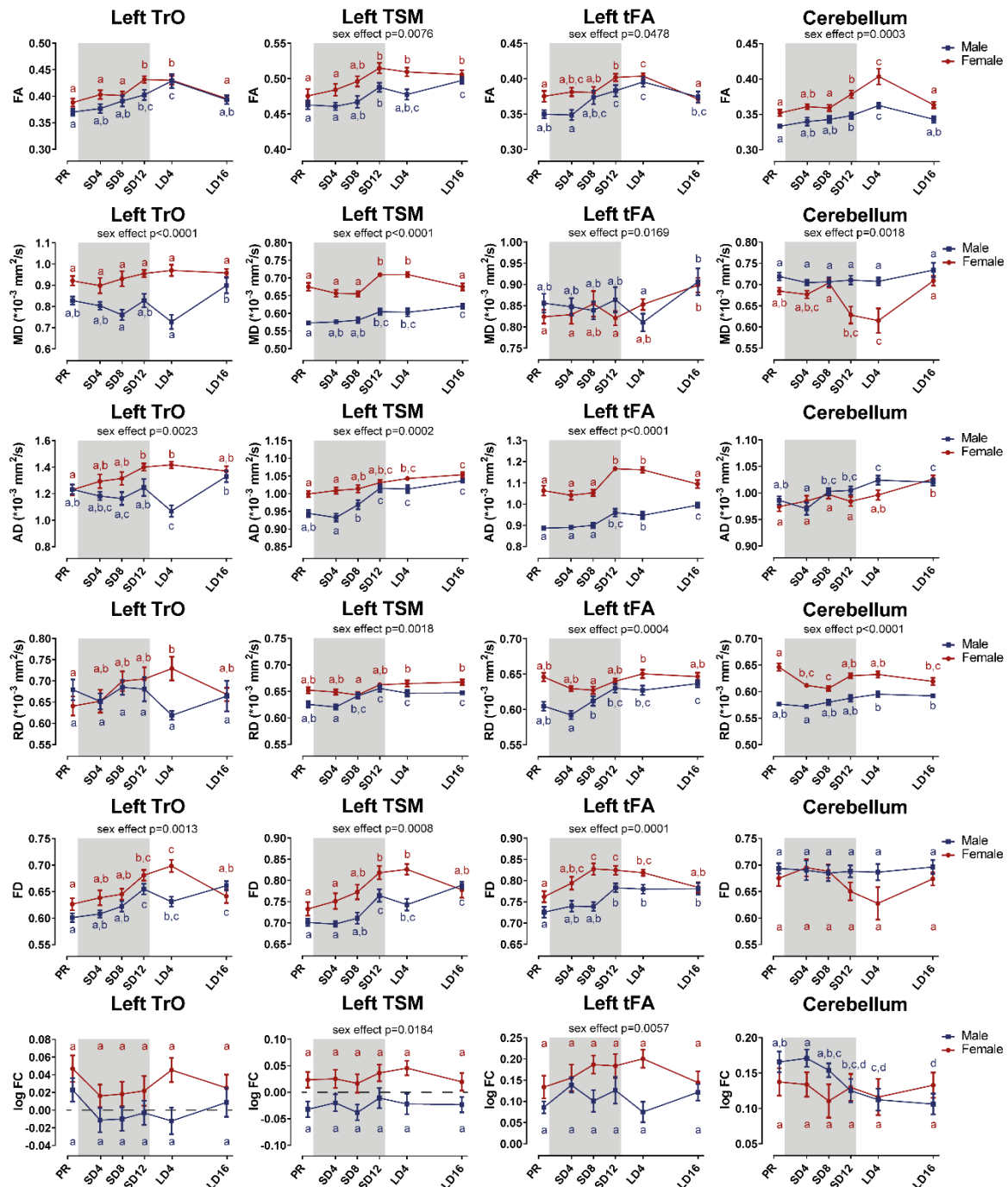
1297
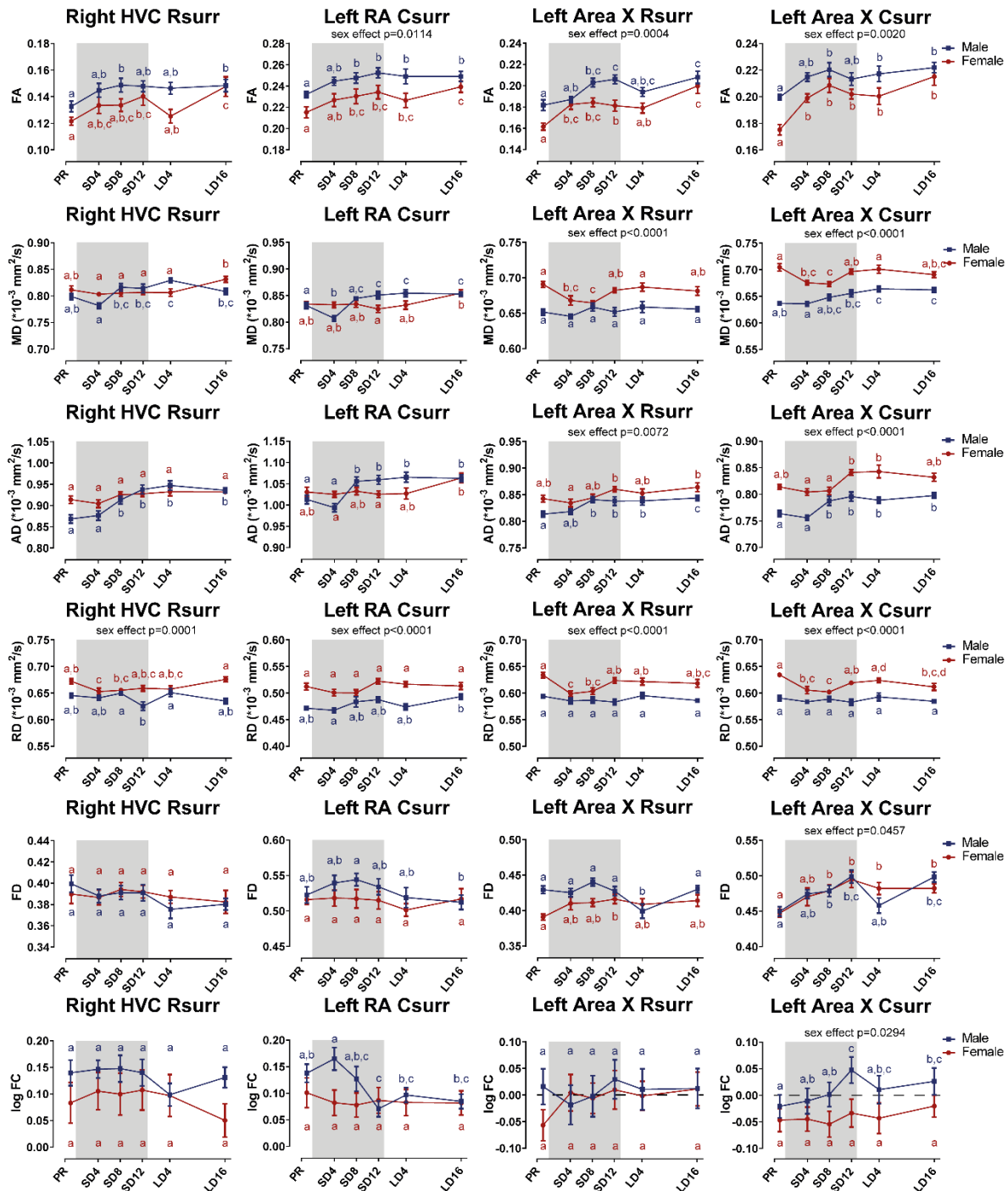
Figure 8 – Figure supplement 2: Summary of significant the longitudinal changes over time in FA, MD, AD, RD, FD and log FC extracted from ROI-based clusters surrounding several song control nuclei including right HVC rostral surroundings (Rsurr), left RA caudal surroundings (Csurr), Area X rostral surroundings and caudal surroundings.

1302

Figure 8 – Figure supplement 3: Summary of the significant longitudinal changes over time in FA, MD, AD, RD, FD and log FC extracted from ROI-based clusters at level of LMAN and several tracts related to song and auditory processing including OM, CSt and LaM.

53

Figure 8 – Figure supplement 4: Summary of the significant longitudinal changes over time in FA, MD, AD, RD, FD and log FC extracted from ROI-based clusters at level of TrO, TSM, tFA and cerebellum.